

Utah State University

DigitalCommons@USU

All Graduate Theses and Dissertations

Graduate Studies

5-1978

A Mathematical Model of Stratified Bi-Directional Flow Through the Railroad Causeway Embankment of Great Salt Lake

James T. Cameron
Utah State University

Follow this and additional works at: <https://digitalcommons.usu.edu/etd>



Part of the [Engineering Commons](#)

Recommended Citation

Cameron, James T., "A Mathematical Model of Stratified Bi-Directional Flow Through the Railroad Causeway Embankment of Great Salt Lake" (1978). *All Graduate Theses and Dissertations*. 3260.
<https://digitalcommons.usu.edu/etd/3260>

This Thesis is brought to you for free and open access by the Graduate Studies at DigitalCommons@USU. It has been accepted for inclusion in All Graduate Theses and Dissertations by an authorized administrator of DigitalCommons@USU. For more information, please contact digitalcommons@usu.edu.



A MATHEMATICAL MODEL OF STRATIFIED BI-DIRECTIONAL FLOW THROUGH
THE RAILROAD CAUSEWAY EMBANKMENT OF GREAT SALT LAKE

by

James T. Cameron

A thesis submitted in partial fulfillment
of the requirements for the degree

of

MASTER OF SCIENCE

in

Engineering

UTAH STATE UNIVERSITY
Logan, Utah

1978

378.2
C145m

ACKNOWLEDGMENTS

The writer would like to express his appreciation to Dr. Gary Z. Watters for his assistance and patience during the long duration of this study.

Appreciation is also extended to the Office of Water Research and Technology for their financial support.

The author would like to express his special gratitude to Charles T. Kincaid for his immeasurable technical aid and overall assistance, without which it would not have been possible to complete this work.

Finally the author would like to thank the total Civil Engineering Department at Utah State University, professors and students included, for making the author's stay here an enjoyable and rewarding experience which will long be remembered.

James T. Cameron

TABLE OF CONTENTS

Chapter	Page
ACKNOWLEDGMENTS	ii
LIST OF TABLES	iv
LIST OF FIGURES	v
ABSTRACT	vii
I INTRODUCTION	1
II LITERATURE REVIEW	6
III THEORETICAL DEVELOPMENT AND NUMERICAL METHODS	13
Seepage Flow Theory	13
Numerical Formulation	15
IV METHOD OF ANALYSIS	31
V RESULTS AND DISCUSSION	37
Two Domain Problem	37
Single Domain Problem	68
VI CONCLUSIONS AND RECOMMENDATIONS	70
LITERATURE CITED	75

LIST OF TABLES

Table	Page
1. Typical ranges of values for dimensionless parameters, . . .	35
2. Variables pertinent to causeway flow collected by Waddell and Bolke (24)	66
3. Permeability calculations deduced from comparison of program flow rate calculations and actual lake values	66

LIST OF FIGURES

Figure	Page
1. Great Salt Lake	2
2. Envisioned flow situation through the causeway	4
3. Boundary conditions on embankment	16
4. Quadratic shape functions along the edge of a single element	21
5. Curvilinear isoparametric quadrilateral element in global x,y and local ξ, η coordinates	22
6. Single domain formulation with boundary specifications	28
7. Approximate and actual variation of velocity across C^0 continuous one-dimensional elements	29
8. Two domain formulation with boundary specifications	30
9. Important variables encountered in this study	33
10. Final construction specifications for Southern Pacific Rail- road causeway fill (from Casagrande (2))	36
11. Visual representation of two domain mesh generated by automatic mesh generator	38
12. Northward flows for highest W/H_1 ratio observed between 1968 and 1972, and $\alpha = 1:1$	40
13. Southward flows for highest W/H_1 ratio observed between 1968 and 1972, and $\alpha = 1:1$	41
14. Northward flows for lowest W/H_1 ratio observed between 1968 and 1972, and $\alpha = 1:1$	42
15. Southward flows for lowest W/H_1 ratio observed between 1968 and 1972, and $\alpha = 1:1$	43
16. Variation of northward flow with W/H_1 ($\alpha = 1:1$)	45
17. Variation of southward flow with W/H_1 ($\alpha = 1:1$)	46
18. The effect of side slope angle (α) on northward discharges	47
19. The effect of side slope angle (α) on southward discharges	48

LIST OF FIGURES (Continued)

Figure	Page
20. Visual representation of flow when $q_s > q_n$ (vertical exaggeration 2x)	51
21. Visual representation of flow when $q_s > q_n$ (vertical exaggeration 2x)	51
22. Visual representation of flow when $q_n > q_s$ (vertical exaggeration 2x)	52
23. Visual representation of flow when $q_n \gg q_s$ and $q_s \approx 0$ (vertical exaggeration 2x)	52
24. Convergence of northward flow rate with iterations	54
25. Convergence of southward flow rate with iterations	55
26. Convergence of maximum density-interface movement with iterations	56
27. Convergence of maximum free surface movement with iterations	57
28. Important variable values and points used in this analysis	59
29. Comparison of constructed model with that of Lin and Lee (17)	63
30. Comparison of constructed model with that of Cheng (4)	64

ABSTRACT

A Mathematical Model of Stratified Bi-directional Flow Through
the Railroad Causeway Embankment of Great Salt Lake

by

James T. Cameron, Master of Science

Utah State University, 1978

Major Professor: Dr. Gary Z. Watters
Department: Civil Engineering

A two-dimensional, finite-element, porous-media flow model is developed to simulate stratified bi-directional flow of brine through the earth embankment carrying the Southern Pacific Railroad across Great Salt Lake. The model is part of a two-year research program whose objective is to develop a computer model of circulation in Great Salt Lake. This overall model is to be used as a predictive device for salinity distributions and circulation patterns in the lake. The porous media flow model is designed to establish flow rates through the Southern Pacific Railroad causeway embankment which traverses the north central part of the lake and divides it into two bodies of water.

The study first develops the mathematical equations which describe two-dimensional stratified bi-directional flow of a fluid through porous media. Next, the problem is numerically posed as a boundary value problem in terms of pressure. This formulation is then solved by an iterative finite element scheme which employs quadratic, isoparametric, quadrilateral elements.

The study also investigates two possible means of performing an analysis of stratified bi-directional flow with a pressure formulation by either posing the problem as a single boundary value problem with two densities of fluid within, or as two single-density boundary value problems coupled at the density interface. The single boundary formulation did not converge with the techniques attempted due to numerical instability at the density interface.

The numerical model developed enables one to calculate fluid flow rates as well as the locations of the free surface and density-interface. The model simulation investigates many lake variables which affect brine flows through the embankment. Realistic model parameters are used which cover the range of actual values observed on the lake for the years 1968 through 1972. The numerical results presented in the study are given in terms of generalized dimensionless variables.

The numerical results appeared to be in agreement with previously performed stratified bi-directional Hele-Shaw model studies. The major lake parameters affecting flow rates through the causeway were the free surface head difference, the southside lake surface elevation and the difference in fluid densities between the upper and lower layers of the embankment. The southward density flow was found to be completely cut off for certain combinations of lake parameters.

Lack of adequate field data collected on the embankment has left both the geometry and the coefficient of permeability of the fill in question, preventing a rigorous verification of the model's ability to predict actual flows. More field data are also necessary to establish whether there is stratification on the north side of the embankment which can greatly affect flow calculations.

A high Reynold's number was found for flow through the embankment, raising a question as to the validity of the Darcian flow assumption used in the analysis. However, the establishment of the true Reynold's number can only be verified through the collection of more empirical data.

(85 pages)

CHAPTER I
INTRODUCTION

In recent times, hydrodynamic flow studies have trended toward computerized analyses. This is due to the many variables involved and the complex nature of their interrelationships as well as the high cost and inflexibility of physical models. This study is part of a two-year research program whose objective is to develop a computer model of circulation in Great Salt Lake. The overall model is to be used as a predictive device for salinity distributions and circulation patterns on the lake. The research work is divided into four parts. The main part will develop circulation patterns, a second models convection-dispersion of a neutrally buoyant tracer, while the other two will develop information to be used as boundary conditions for the circulation model. This study establishes flow rates through the porous media of the Southern Pacific Railroad causeway embankment which traverses the north central part of the lake and divides the lake into two bodies of water as shown in Figure 1.

Because the Great Salt Lake is a terminal lake, all the salinity which enters the lake basin remains there, except for that mined. This geomorphic phenomenon has made the lake an ideal site for extracting minerals for industrial purposes. Therefore, an account of the quantity of minerals in the north and south arm brines, and the exchange of the brines through the causeway fill has become a major concern in this and previous Great Salt Lake studies.

The emplacement of the 12-mile long causeway fill in 1957 has apparently upset the natural salinity balance of the lake (Adams (1)). The

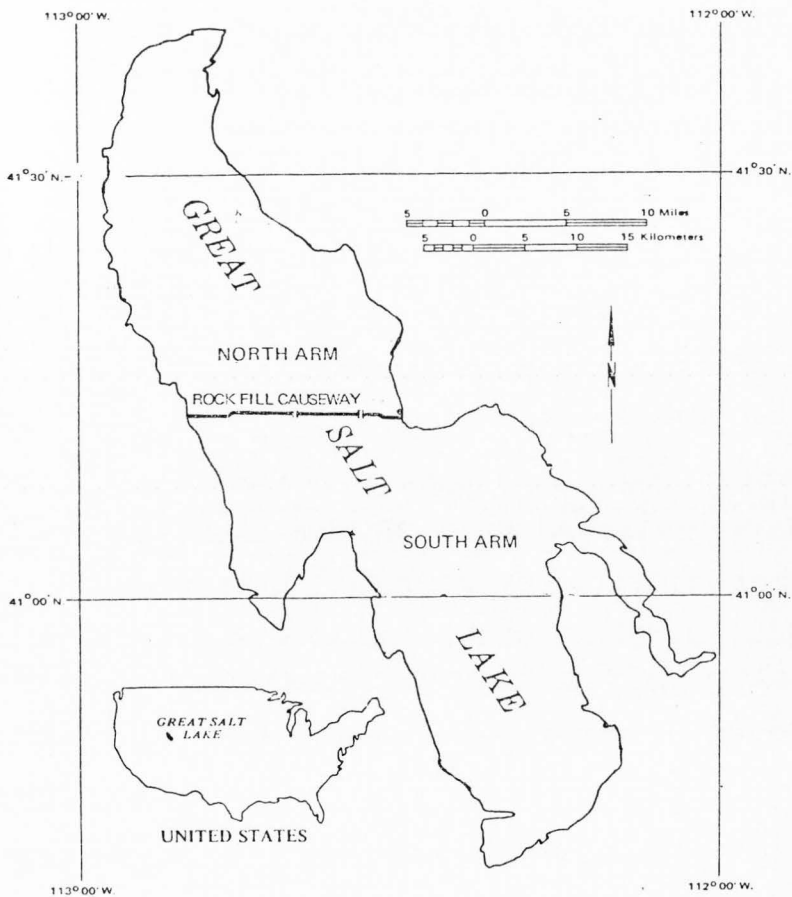


Figure 1. Great Salt Lake

brines in the northern portion of the lake have been observed to remain near saturation, while those in the southern section have become more dilute. The southern arm is also stratified vertically into two layers of differing brine density. Also, because the majority of surface inflow to the lake is into the southern section, its surface elevation has been observed to be as much as 2.3 feet higher than that of the north. Because the embankment (including two 15-foot culverts) serves as the only means whereby the north and south arms can exchange brines, an understanding of its effect on the lake waters has become a major concern in this and previous studies of the lake. Tracer studies, field observations, and measurements taken on the embankment have indicated that the flow within it is both stratified and bi-directional. Figure 2 depicts a two-dimensional view of the envisioned flow situation through the embankment.

This research first develops the mathematical equations which describe stratified bi-directional flow such as that occurring through the causeway embankment. Next, the problem is numerically posed as a boundary value problem. This formulation is then solved by an iterative finite element scheme which employs quadratic isoparametric quadrilateral elements. The numerical model developed enables one to calculate the fluid flow rates as well as the locations of the free surface and density-interface. Realistic model parameters are used which cover the range of the actual values observed on the lake for the years 1968 through 1972. The numerical results presented in this study are given in terms of generalized dimensionless variables. The numerical results derived in this study cannot be confidently interpreted as quantitative values of the actual flow through the causeway of Great Salt Lake. Inadequate field data collected

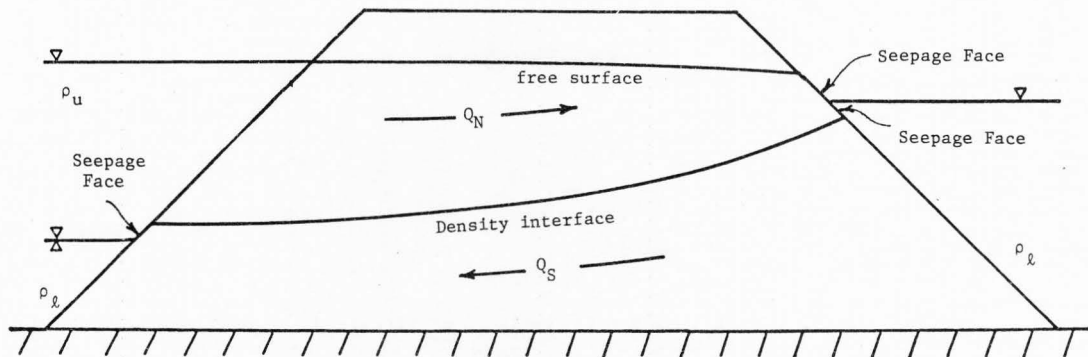


Figure 2. Envisioned flow situation through the causeway,

on the embankment has left both the geometry and the coefficient of permeability in question. Since these factors are very instrumental in predicting causeway flows, a rigorous verification of the model's ability to predict actual lake flows could not be performed.

This model assumes no stratification of lake waters on the north side of the fill. It is shown that this assumption greatly reduces flow rates through the embankment. More data are also necessary to determine whether stratification does, indeed, exist on the north side.

CHAPTER II
LITERATURE REVIEW

The investigation of unconfined seepage flow problems has a long history. Because the location of the phreatic surface (and interface in stratified flow) is unknown, one cannot formulate a complete boundary value problem; therefore some sort of iterative scheme is necessary to lead to a solution. It is the various approaches to this approximating process which give rise to the variety of techniques available today.

Most analyses of seepage problems assume that flow is incompressible and that Darcy's law is applicable. These assumptions suggest the introduction of a potential function which greatly simplifies groundwater flow analyses. Substitution of Darcy's law into the incompressible continuity equation leads directly to Laplace's equation, $\nabla^2\phi = 0$, where ϕ is the potential function. For homogeneous, isotropic media whose interior flow is described by Laplace's equation, equipotential lines and streamlines form an orthogonal network. This is the basis for the flow net method (3) which is widely used for engineering purposes.

Flow problems have been studied using both physical and analog models. In a physical model the prototype is scaled to a workable size through similitude techniques (18). The scaled model is then used to obtain information in the form of dimensionless variables which can be interpreted for the prototype. Analog models solve a given problem in a completely different physical system which obeys the same differential equations under similar boundary conditions. For instance, there is a mathematical analogy between potential flow and the electric field of a direct current.

Herbert (13) used this fact to model time variant flow. The use of both types of models for flow analysis is limited for a number of reasons--they can be expensive to construct; accurate measurements are difficult to obtain; and changing a model for optimization in design can be a difficult and time consuming task.

In recent times, with the advent of the digital computer, the object of major efforts in porous media flow studies has been in the area of numerical analysis. Finite difference techniques were developed for both inverse and direct formulations of porous media flow problems. For example, in inverse formulations, Jeppson (15) treats various homogeneous, isotropic (and/or anisotropic) examples by a transformation to the complex potential plane where the x and y coordinates are the dependent variables and the stream (Ψ) and potential (Φ) functions are the independent variables. The advantage of this approach is that the free surface boundary condition is known in the complex plane since, in a steady flow, it is a streamline. However, it is still necessary to use some kind of iteration scheme to solve the problem. Once formulated in the complex plane, which is rectangular for common seepage problems the domain is subdivided into a grid of rectangles, the corners of which are called nodes. A finite difference form of Laplace's equation in terms of Ψ and Φ is applied at each of these nodes to solve the problem in the complex plane. The Cauchy-Riemann equations are used to convert back to the physical plane.

A typical example of the direct formulation of a seepage flow problem was done by Finnemore and Perry (9) using reduced pressures, $P = p/\rho g$, where P is the reduced pressure head, p is the real pressure, ρ is the mass density, and g is the gravitational constant. They assumed the

location of the free surface, then moved it based on whether the free surface boundary conditions were met for that configuration (i.e. $p =$ atmospheric, normal velocity = 0).

In a finite difference approach the problem domain is represented by a number of points, or nodes, arranged quadrilaterally and orthogonally within the domain. Various operators are then applied using the nodal values surrounding a particular node of interest to numerically solve a boundary value problem. In a finite element approach the problem domain is subdivided into a number of elements. The modeling variable is allowed to assume a specified variation across elements to determine the solution field. The elements are not restricted to being rectangular as with the finite difference approach. They can be triangular, rectangular or even curvilinear in the physical plane. The value of the dependent variable in an element is based both on the specified variation across the element and on the values of the variable at the nodal points used to describe a given element.

In a finite element approach one can also formulate a problem in either the complex or the physical plane. Shaug and Bruch (22) developed an inverse formulation similar to Jeppson's with the added attraction that the streamlines and equipotential lines could be separated by arbitrarily selected increments in the complex plane. The algorithm used allowed one to concentrate equipotential and streamlines in high velocity regions.

Direct formulation using finite elements has been performed in a number of studies (6, 11, 19, 23). As in the direct finite difference approach to such problems, generally the free surface location is assumed and then adjusted based on whether or not it satisfies the boundary

The majority of the methods applied to solving unconfined seepage problems have been directed to solving single density flow situations. However, this study will involve the case of a two-density flow. There has been little numerical work done in this area. Lin and Lee (17) performed a Hele-Shaw model study directed toward application to the causeway of Great Salt Lake. Cheng (4) performed a finite element analysis of two-density flow by separating the investigation into two single-density phases. The two phases were coupled at the interface using the criteria that at the final location of the interface the pressures calculated from the upper and lower phases should be equal. Cheng's modeling parameter is piezometric head and quadratic, isoparametric, quadrilateral elements were used to subdivide the two domains. He adjusted the free surface in the standard way by assuming its geometry and iterating based on whether the necessary boundary conditions were met for that chosen geometry. Cheng's results are somewhat misleading. His final results indicate that for bi-directional flow through an earth embankment the upper density flow is continually less than the lower density flow regardless of the boundary conditions or the problem parameters. In application to bi-directional, stratified flow through the railroad embankment of Great Salt Lake this cannot be the case. The majority of inflow to the lake is into the portion south of the embankment. So, the north section has to receive most of its inflow through the causeway. This appears to be in direct contradiction to Cheng's results which imply that the flow toward the south is greater. His results appear to be dependent on the unrealistic dimensions chosen to represent his modeling domain.

Pinder and Gray (21) point out the importance of obtaining a continuous velocity distribution when a solution to a transport equation is sought in a region of highly variable flow. They suggest two means of obtaining this end:

1. To use a basis function which has continuous first derivatives across element boundaries, or
2. To formulate a four-equation scheme which treats flux as well as potential as an independent variable.

They describe the process for the second method. Three equations for flow in the x, y and z directions and one which assures continuity of mass are formulated to model an example problem. They point out two undesirable properties inherent with this method. First, the stiffness matrix is unsymmetric which means more computer storage is required to solve a problem than with other approaches. Second, the stiffness matrix contains zero elements along its diagonal which leads to difficulties in applying many of the equation solving schemes because most schemes pivot on diagonal elements.

There are advantages and disadvantages in any of the above methods of solving unconfined seepage flow problems. The finite element technique has shown great promise in recent years because of its versatility in dealing with non-homogeneous and anisotropic cases, by its ability to model irregular geometries while still being formulated in the physical plane, and, once a model is constructed, by its portability to a variety of different problems. Some of the techniques used in the other methods can be applied to a finite element analysis. This work will attempt to take advantage of these previous studies in solving stratified, bi-directional,

porous media flow problems which can be applied to the railroad embankment in Great Salt Lake.

CHAPTER III

THEORETICAL DEVELOPMENT AND NUMERICAL METHODS

Seepage Flow Theory

For two-dimensional, steady flow through uniform media, Darcy demonstrated that the seepage velocity was proportional to the gradient of the total head.

$$v_s = -k \, dh/ds \quad (3.1)$$

where s is the direction of flow, k is defined as the coefficient of permeability dependent on the properties of both the fluid and the soil,

$$h = p/\rho g + y \quad (3.2)$$

where p is the pressure, ρ is the mass density of fluid, g is the gravitational constant, and y is the vertical distance above some datum. Darcy's law includes any variation in fluid viscosity within the k term.

For two-dimensional flow,

$$u = -k_x \, \partial h/\partial x \quad \text{and} \quad v = -k_y \, \partial h/\partial y \quad (3.3)$$

for flow in the x and y coordinate directions, respectively. Coupling them with the continuity equation for two-dimensional flow,

$$\partial u/\partial x + \partial v/\partial y = 0 \quad (3.4)$$

the following equation results for constant k_x and k_y .

$$k_x \, \partial^2 h/\partial x^2 + k_y \, \partial^2 h/\partial y^2 = 0 \quad (3.5)$$

When Equation 3.5 is applied throughout a specified problem domain, the analysis becomes a boundary value problem.

In a two-density porous media flow problem, piezometric head is not continuous across the density interface. This would preclude the analysis of this problem type as a single boundary value problem thereby forcing

one to perform the analysis as two boundary value problems, each with a constant density of fluid. However, if the governing differential equations are formulated in terms of pressure, this limitation can be circumvented. Pressures are continuous across a density interface enabling one to formulate a two-density flow analysis as a single boundary value problem. In terms of pressure, Equation 3.5 takes the form

$$k_x \frac{\partial^2 (p/\rho g + y)}{\partial x^2} + k_y \frac{\partial^2 (p/\rho g + y)}{\partial y^2} = 0 \quad (3.6)$$

This is the differential equation which will be used to represent flows in this model study.

It is necessary for the solution of Equation 3.6 to satisfy certain boundary conditions to properly represent a given problem. There are basically two types of boundary conditions involved with the solution of equations of the form found in Equation 3.5. One type deals with the values of the field variable along the domain boundaries, while the other type deals with the normal derivative values of the field variable.

A Dirichlet condition is a boundary condition where the field variable value is known on the boundary. If this value is zero, the condition is termed a homogeneous Dirichlet boundary. If it is a non-zero constant, it is called a non-homogeneous Dirichlet boundary. A Neumann boundary condition is one in which the normal derivative of the field variable at the boundary is forced to take on a given value. These, too, can be both homogeneous and non-homogeneous. Neumann boundaries describe the normal velocity, V_n , (and flux) conditions across boundaries in seepage flow problems.

The equations of flow and the boundary conditions are depicted in Figure 3 for the pressure formulation of a two-density porous media flow problem. On the free surface Neumann and Dirichlet conditions hold, i.e., $V_n = 0$ and $p = \text{atmospheric}$, respectively. The static pressure of the overlying fluid forms the Dirichlet condition along the sides of the domain, while both the density interface and the base of the domain must satisfy the homogeneous Neumann condition (i.e. $V_n = 0$).

Numerical Formulation

Galerkin approximation

Let the function, $L(p)$, be defined as

$$L(p) = k_x \frac{\partial^2 (p/\rho g + y)}{\partial x^2} + k_y \frac{\partial^2 (p/\rho g + y)}{\partial y^2} \quad (3.7)$$

In general format Equation 3.6 can be written in the form

$$L(p) - f = 0 \quad (3.8)$$

where f^* is a known function of the independent variables, also called a forcing function.

To solve Equation 3.8 numerically, the method of weighted residuals (8,20) will be employed. In this method an approximate solution set, p' , is chosen to represent the exact solution set, p . These approximations shall be called trial functions and are formed from a set of basis monomials which describe the space of functions chosen to approximate the exact solution. The p' functions must satisfy both the differential Equation 3.8 and the boundary restrictions placed on a given problem.

*In this analysis $f = 0$, since infiltration and evaporation are considered negligible. The general notation, however, will still be retained.

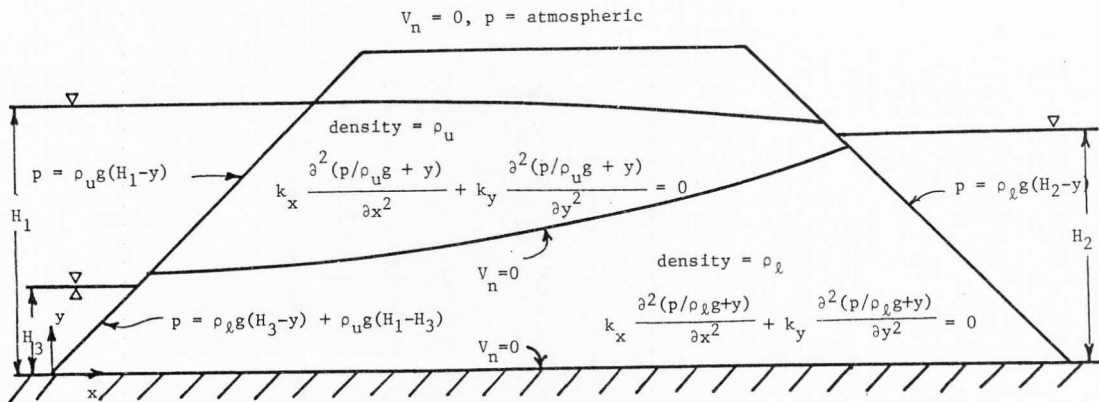


Figure 3. Boundary conditions on embankment.

When p' is substituted for p in Equation 3.8 it is unlikely that the equality will still hold. Instead, there is likely to be some residual due to the inexactness of the trial functions chosen, that is,

$$L(p') - f = R \quad (3.9)$$

where R is the residual. The method of weighted residuals orthogonalizes the residual to an arbitrarily selected set of weight functions by taking the inner product of Equation 3.9 with the chosen set of weighting functions, W_i .

$$\langle W_i, L(p') - f \rangle = \int_{\Omega} [L(p') - f] W_i \, d\Omega = 0 \quad (3.10)$$

where $\langle u, v \rangle = \int_{\Omega} u \cdot v \, d\Omega$ is the inner product of u with v . The Galerkin form of the method of weighted residuals results if the monomial basis of the weighting functions, W_i are the same as those chosen to approximate p , the solution.

Finite element method

The preceding discussion referred to the total domain of a particular problem. Since Equation 3.9 holds for any single point in the solution domain, it holds equally well for any collection of points defining an arbitrary sub-domain or element of the whole domain. The finite element method takes advantage of this fact by discretizing the whole domain into a number of elements. This method can be applied only if the trial functions used to represent the approximate solution, p' , are chosen so as to satisfy certain completeness and compatibility requirements (14). These insure both a continuity across the solution domain of the approximating variable and enable one to analyze the entire domain as a union of

subdomains. Essentially, they guarantee that the equations developed will be integrable.

The solution to Equation 3.10 now becomes a solution of summations over individual elements.

$$\int_{\Omega} [L(p') - f] W_i d\Omega = \sum_{e=1}^r \int_{\Omega(e)} [L(p') - f] W_i d\Omega = 0,$$

$$i = 1, 2, \dots, q \quad (3.11)$$

where (e) implies an element equation, r is the total number of elements which comprise the domain and q is the number of weight functions employed.

For the moment, consider only one element of the domain, keeping in mind that, eventually, each element contributes to formulating the problem as a whole. Each element is defined by a given number of points (nodes) dependent on both the geometry of the elements one wishes to model and the degree of continuity chosen to approximate the solution domain.

The suitability of the Galerkin method to accurately approximate the exact solution, p, stems from the proper choice of the trial functions. Efficient numerical approximations can be achieved by choosing piecewise continuous polynomials as the trial functions. Polynomials are normally chosen because they represent the simplest form for an approximating function and can be easily integrated and differentiated. These functions are chosen to represent the field variable, p', in Equation 3.11.

$$p' = \sum_{i=1}^n P_i N_i, \quad (3.12)$$

where n is the number of nodes chosen to define an element, N_i is a set of trial functions expressed in terms of the nodal coordinates, and p_i is the set of n discrete nodal values of p' associated with the given element.

Coordinate transformation

The necessary integrations required to solve the element equations defined in 3.11 will generally be in a form too complex to integrate exactly. This is due to the variety of shapes and sizes elements may have within the whole domain. Therefore, except for very simple problems, it becomes necessary to perform the integrations numerically. To aid in this numerical integration it is sometimes more convenient to derive the element characteristics in a dimensionless, normalized, termed "natural" coordinate system, and find the transformation equations which map each physical element onto the standard element. For two dimensions, the inverse transformation (i.e. mapping from the natural coordinate system to the x, y coordinate system) is of the form

$$x = \sum_{i=1}^n M_i(\xi, \eta) x_i \quad \text{and} \quad y = \sum_{i=1}^n M_i(\xi, \eta) y_i, \quad (3.13)$$

where $M_i(\xi, \eta)$ are the mapping, or shape functions, in terms of ξ and η , which relate the two domains via the nodal values, x_i and y_i .

Shape functions and trial functions are identical in concept in that they both serve as a means of interpolating or representing a given variable. This discussion will use the term shape function when referring to coordinate transformations and modeling geometries, while trial functions will be used in relation to the field variable representations.

A transformation must be unique, that is, for each point in one system there must be one, and only one, corresponding point in the other system. If this is not the case, elements may be violently distorted and fold back on themselves creating serious problems in obtaining accurate numerical approximations in a given problem.

The choice of shape functions used to construct elements is dependent on maintaining the continuity conditions in the real, or global coordinate system. The shape functions are chosen in such a way that M_i is unity at node i and zero at all other nodes in the element. Recalling that if the approximating polynomial is of the form described in Equation 3.12, it follows that the undetermined coefficients, p_i , which are approximated, will be the required function, p^i at the n nodal points.

If, within an element, the shape functions used to represent the problem geometry are chosen to have the same order as the trial functions that are used to model the field variable (i.e. $M_i = N_i$), the element is said to be isoparametric. In comparison, subparametric elements are elements whose geometry is described by a lower-order polynomial than that used to model the field variable, and superparametric elements are those which use a higher-order polynomial. The compatibility and completeness of the solution employing isoparametric elements is guaranteed provided the original trial functions were compatible and complete. The employment of isoparametric elements has the added attraction of enabling one to map elements with curved sides, as well as linear sides, onto a standard element in the natural coordinate system.

Quadratic shape functions shall be employed in this two-dimensional analysis. Figure 4 depicts a typical set of quadratic shape functions

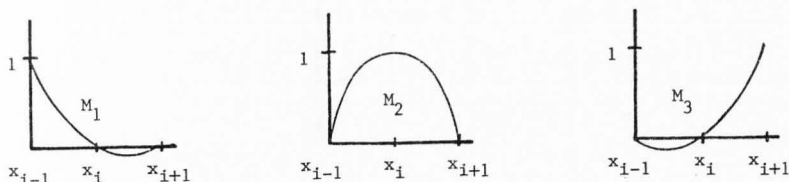


Figure 4. Quadratic shape functions along the edge of a single element.

along an interval (x_{i-1}, x_{i+1}) for a two-dimensional domain. Note that the shape function of a particular node has a value of one at the node and zero at the other two nodes and varies quadratically between nodes. These particular shape functions are called C^0 continuous indicating that they only guarantee continuity of the approximate solution across element boundaries up to the zeroth derivative. It is also possible to formulate shape functions which guarantee continuity up to the m^{th} derivative across element boundaries while guaranteeing $(m+1)$ derivative continuity within elements. Such shape functions are called C^m continuous.

The geometry of the elements used to represent a domain is somewhat problem dependent. In two-dimensional problems triangular or quadrilateral shapes are used, the sides of which can vary linearly, quadratically, etc., dependent on the degree of curvature one wishes to allow the elements to take. It should be noted, however, that higher order elements require more complicated and time consuming solutions which increase computational costs. In deciding whether to use higher order elements one must weigh the improved quality of the solutions against the increased

computational costs. The continuity requirements of the representative functions must also be maintained.

This study will incorporate an isoparametric quadrilateral element using quadratic C^0 continuous shape functions, also called an eight-node serendipity element. This element has been shown to be highly efficient in modeling irregular domains for two-dimensional problems (7). The standard element in the natural coordinate system is square with corner coordinates of $(-1,1)$, $(1,1)$, $(-1,-1)$, and $(1,-1)$. Figure 5 shows how an eight node serendipity element in the x,y coordinate system would map to the natural coordinate system of ξ, η .

In general, the integral equation for an element in a given problem will have the form

$$\int_{\Omega(e)} F(p, \partial p/\partial x, \partial p/\partial y) dx dy \quad (3.14)$$

Since $p(x,y)$ is expressed as a function of ξ and η it is necessary to describe $\partial p/\partial x$, $\partial p/\partial y$, and $dx dy$ in terms of ξ and η . By the chain rule of differentiation

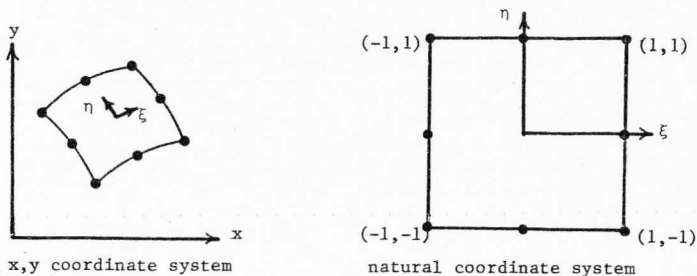


Figure 5. Curvilinear isoparametric quadrilateral element in global x,y and local ξ, η coordinates.

$$\begin{aligned} dp/d\xi &= \partial p/\partial x \partial x/\partial \xi + \partial p/\partial y \partial y/\partial \xi \text{ and } dp/d\eta = \partial p/\partial x \partial x/\partial \eta + \\ &\partial p/\partial y \partial y/\partial \eta \end{aligned} \quad (3.15)$$

These can be combined in matrix form as:

$$\begin{bmatrix} p, \xi \\ p, \eta \end{bmatrix} = \begin{bmatrix} x, \xi & y, \xi \\ x, \eta & y, \eta \end{bmatrix} \begin{Bmatrix} p, x \\ p, y \end{Bmatrix} = [J] \begin{Bmatrix} p, x \\ p, y \end{Bmatrix}, \quad (3.16)$$

where $u,_{t}$ implies the derivative of u with respect to t , and $[J]$ is the Jacobian of the transformation,

$$[J] = \begin{bmatrix} x, \xi & y, \xi \\ x, \eta & y, \eta \end{bmatrix} = \begin{bmatrix} N_{1,\xi} & N_{2,\xi} \cdots N_{n,\xi} \\ N_{1,\eta} & N_{2,\eta} \cdots N_{n,\eta} \end{bmatrix} \begin{bmatrix} x_1 & y_1 \\ x_2 & y_2 \\ \vdots & \vdots \\ x_n & y_n \end{bmatrix} \quad (3.17)$$

in which (x_i, y_i) are the cartesian coordinates of an element described by n nodal points. Note that the differentiations of x and y are performed on the shape functions with which they are approximated. That is, for example,

$$x, \xi = \{N_{i,\xi}\}^T \{x_i\}, \quad (3.18)$$

where $\{\}^T$ implies a row matrix and $\{\}$ implies a column matrix. Expressions for $\partial p/\partial x$ and $\partial p/\partial y$ can be derived by inverting Equation 3.16.

$$\begin{Bmatrix} p, x \\ p, y \end{Bmatrix} = \begin{bmatrix} N_{1,x} & N_{2,x} & \cdots & N_{r,x} \\ N_{1,y} & N_{2,y} & \cdots & N_{r,y} \end{bmatrix} \begin{Bmatrix} p_i \end{Bmatrix} = [J]^{-1} \begin{bmatrix} N_{1,\xi} & N_{2,\xi} & \cdots & N_{r,\xi} \\ N_{1,\eta} & N_{2,\eta} & \cdots & N_{r,\eta} \end{bmatrix} \begin{Bmatrix} p_i \end{Bmatrix} \quad (3.19)$$

The only other information required to perform the necessary integrations in the natural (or local) coordinate system is to replace the differential area $dxdy$ by

$$dxdy = |J|d\xi d\eta \quad (3.20)$$

where $|J|$ is the determinant of the Jacobian in terms of ξ and η . It is also necessary to change the limits of integration to plus to minus one in both directions (for quadrilateral elements in two dimensions). Thus, Equation (3.14) is now

$$\int_{-1}^1 \int_{-1}^1 F \left[p(\xi, \eta), \quad \partial p / \partial \xi, \quad \partial p / \partial \eta, \quad [J]^{-1} \right] |J| d\xi d\eta \quad (3.21)$$

The integration is performed by a Gaussian quadrature technique.

This procedure integrates a one-dimensional polynomial of degree $2N-1$ exactly by weighting the value of the function at N particular specified points, called Gauss points. Since each element is mapped onto a standard element, the same Gauss points and weights in the natural element can be used for every element. All that is necessary is to evaluate the integrand at the Gauss points and weight them properly.

$$\int_{\Omega} F(\xi) d\xi = \sum_{i=1}^N w_i f(\xi_i), \quad (3.22)$$

where w_i are the weights and ξ_i are the Gauss points. The two-dimensional form of this procedure is

$$\int_{\Omega} F(\xi, \eta) d\xi d\eta = \sum_{i=1}^N \sum_{j=1}^N w_i w_j f(\xi_i, \eta_j). \quad (3.23)$$

Finite element representation

It is now possible to return to the original differential equation (Equation 3.6) and derive its finite element form to be used in modeling potential flow.

$$k_x \frac{\partial^2 (p/\rho g + y)}{\partial x^2} + k_y \frac{\partial^2 (p/\rho g + y)}{\partial y^2} = 0 \quad (3.6)$$

The Galerkin method of weighted residuals is now applied to the element form of equation of (3.6). In this method the weight functions, W_i , are identical to the trial functions, N_i . The separate representations will be retained, however, to better illustrate the finite element representation process and the parts played by the weighting and shape functions.

$$\sum_{e=1}^r \int_{\Omega(e)} \left[k_x W_i \frac{\partial^2 (p'/\rho g + y)}{\partial x^2} + k_y W_i \frac{\partial^2 (p'/\rho h + y)}{\partial y^2} \right] dx dy = 0$$

(i = 1, 2, ..., q) (3.24)

where W_i are the set of weight functions and p' implies an approximate solution of the exact solution, p .

Unnecessary continuity conditions can be avoided by reducing the order of differentiation of the integrand. Green's Second Identity is applied to Equation 3.24 to give

$$\sum_{e=1}^r - \int_{\Omega(e)} k_x W_{i,x} h'_{,x} + k_y W_{i,y} h'_{,y} dx dy + \int_S(e) W_i (k_x \ell_x h'_{,x} + k_y \ell_y h'_{,y}) dS = 0, \quad (3.25)$$

where ℓ_x and ℓ_y are the direction cosines of the outward directed normal.

Substituting $h = (p/\rho g + y)$ gives

$$\sum_{e=1}^r - \int_{\Omega(e)} \left[k_x W_{i,x} p_{,x} / \rho g + k_y W_{i,y} (p_{,y} / \rho g + 1) \right] dx dy + \int_S(e) (k_x W_{i,x} p_{,x} / \rho g \ell_x + k_y W_{i,y} p_{,y} / \rho g \ell_y + k_y W_{i,y} \ell_y) dS = 0 \quad (3.26)$$

Since each individual element is assumed homogeneous in k_x , k_y and ρ ,

$$\sum_{e=1}^r - \int_{\Omega(e)} (k_x W_{i,x} p_{,x} + k_y W_{i,y} p_{,y} + k_y W_{i,y} \rho g) dx dy + \int_S(e) (k_x W_{i,x} p_{,x} \ell_x + k_y W_{i,y} p_{,y} \ell_y + k_y W_{i,y} \rho g \ell_y) dS = 0 \quad (3.27)$$

This is the equation in two dimensions which must be numerically integrated to model potential flow problems which employ pressure as the independent variable.

The second integral in Equation 3.27 is called the natural boundary condition. This term, in the form stated above, is the Neumann condition along an exterior boundary. Excluding this term along a given boundary, setting it equal to zero, forces a homogeneous Neumann condition along that boundary. This, in effect, states that the normal velocity (and flux) at that boundary is zero. This study will not incorporate flux specifications, therefore, the natural boundary term can be neglected.

Keeping the above in mind, if Equation 3.27 is written in matrix form in terms of trial functions, where $p^{(e)} = \{N_i\}^T \{p_i\}$ and the Galerkin method is applied (i.e. $\{W_i\} = \{N_i\}$), the following equation results.

$$\sum_{e=1}^r - \int_{\Omega(e)} \left[k_x \{N_{i,x}\} \{N_{j,x}\}^T + k_y \{N_{i,y}\} \{N_{j,y}\}^T \right] dx dy \{p_j\} + \int_{\Omega(e)} k_y \rho g \{N_{i,y}\} dx dy = 0 \quad (i, j = 1, 2, \dots, q) \quad (3.28)$$

For the total domain Equation 3.28 takes the general form

$$\left[A_{k\ell} \right] \{p_\ell\} = \{B_k\}, \quad (k, \ell = 1, 2, \dots, q) \quad (3.29)$$

where

$$\left[A_{k\ell} \right] = \sum_{e=1}^r \int_{\Omega(e)} k_x \{N_{i,x}\} \{N_{j,x}\}^T + k_y \{N_{i,y}\} \{N_{j,y}\}^T dx dy$$

and

$$\{B_k\} = \sum_{e=1}^r \int_{\Omega(e)} \rho g \{N_{i,y}\} dx dy .$$

Both $\left[A_k \right]$ and $\{B_k\}$ are global arrays formulated from amassing the individual element information while r is again the total number of elements subdividing the whole domain and q is the total number of nodes representing the domain. Equation 3.28 then, describes a system of q equations and q unknowns which can be numerically solved for the $\{p_j\}$ nodal values.

In this formulation $\left[A_{k\ell} \right]$ is symmetric and banded. These two properties vastly reduce the computer storage of $\left[A_{k\ell} \right]$ necessary in solving the system of linear equations because only the unique values of the matrix are important to perform the solution. A Cholesky square root solution technique is employed to solve the system for the q unknowns.

Iteration technique

As mentioned previously, the problem of stratified bi-directional potential flow cannot be formulated explicitly because the locations of the free surface and density interface are not known a priori. However, it is known that both of these surfaces must satisfy the homogeneous Neumann boundary condition. It is also known that pressure must be continuous across the interface and that pressure on the free surface is atmospheric. The final solution can then be found by (1) assuming locations of these two surfaces, (2) enforcing either the Neumann or the Dirichlet condition applicable to each surface and (3) adjusting the free surface and density interface based on how well the other applicable boundary condition is met. This procedure is repeated until a desired tolerance is met.

There are two schemes possible for solving this problem with a pressure formulation. The first scheme is to model the problem as a single domain with the interface delineated as a string of element edges (Figure 6). In this formulation the pressure continuity on the interface

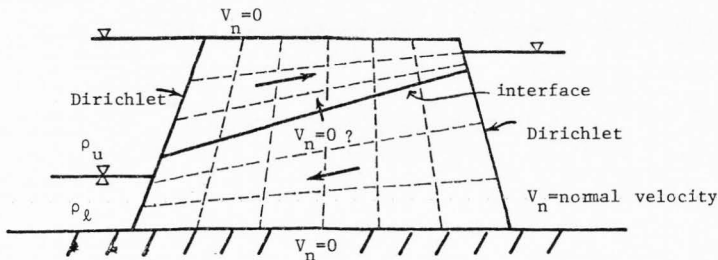


Figure 6. Single domain formulation with boundary specifications.

is automatically met. So the solution technique must be keyed to whether or not the Neumann condition is met along this surface. Because velocities are derivative properties and only C^0 continuous elements are used, it is questionable whether this method can converge to a unique solution.

Figure 7 shows what occurs between the actual and approximate solutions for velocity using C^0 continuous elements in a one-dimensional grid. The velocity over the whole element is continuous, but will not generally be continuous between elements. This fact may prevent the problem from converging when represented as a single domain.

The second scheme is similar to that used by Cheng (4) except that the modeling parameter will be pressure rather than piezometric head. The problem domain is divided into two constant-density regions as shown in Figure 8.

The homogeneous Neumann boundary is effective along the upper and lower boundaries for both regions. This natural boundary condition is automatically met along these surfaces for both regions when Equation 3.28

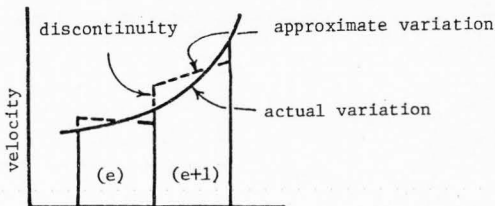


Figure 7. Approximate and actual variation of velocity across C^0 continuous one-dimensional elements.

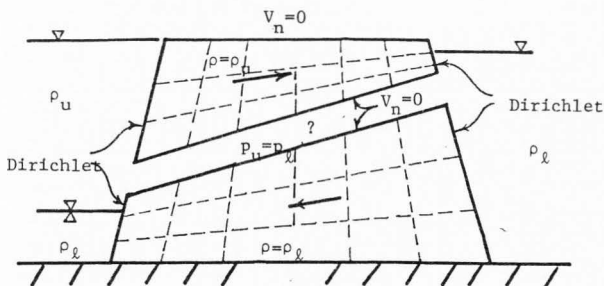


Figure 8. Two domain formulation with boundary specifications.

is used to formulate the element equations. The testing criteria for the density interface is whether or not the pressures in the upper (ρ_u) and lower regions (ρ_l) are equal along the corresponding boundaries. The Dirichlet boundary conditions along the sides for both schemes are simply the static pressures of the overlying fluid at a given side node.

Each element must have a constant density, ρ , and a constant permeability in the x and y directions, k_x and k_y , respectively. Also, since little is known of the permeability properties of the causeway fill to which this model will be applied, isotropic permeabilities are assumed. Anisotropy, however, is introduced with the only restriction that the local coordinate axes must coincide with the major and minor permeability axes.

CHAPTER IV
METHOD OF ANALYSIS

A model was designed to determine flow rates in both the upper and lower regions of flow (Q_N and Q_S in Figure 2) based on a specified domain geometry, element properties, and certain boundary condition information. Recall that an initial assumption must be made as to the locations of the free surface and interface by placing them along element edges. Permeabilities and fluid density for each element are also required. The boundary condition information necessary includes the upstream and downstream free surface and interface elevations. The above information fully describes a given steady state flow problem from which a unique set of flow rates to a stratified, bi-directional problem can be calculated.

The parameter information for this study was taken from Waddell and Bolke (24) which contained lake elevation and specific gravity information for Great Salt Lake for the years 1968 through 1972. The report did not provide enough information to be used in a rigorous verification of the model, so until more complete data is collected one must be satisfied with qualitative and rough quantitative verifications only.

Dimensional analysis

There are many parameters influencing this problem making any relationships between the variables somewhat complex. A dimensional analysis was performed in order to more clearly present the results. This process combines the problem variables in such a way as to form a set of non-dimensional parameters (i.e. unitless or pure numbers). These dimensionless

parameters are then used in plotting the results of the analysis. For a more complete explanation of this procedure, see Murphy (18).

The fundamental variables for this problem are:

- ρ_l - fluid density in lower section of fill (slug/ft³)
- $\Delta\rho$ - fluid density difference between upper and lower sections of fill (slug/ft³)
- H_1 - depth of lake surface on south side of embankment (ft)
- ΔH - difference in surface elevation between north and south sides of embankment (ft)
- H_3 - depth of interface in southern portion of lake (ft)
- k - permeability of soil (to reduce number of parameters permeability is assumed isotropic and homogeneous throughout domain--ft/sec)
- W - width of base of domain of flow (ft)
- q_s, q_n - flow rates per unit thickness through the fill in the south and north directions, respectively. (ft³/sec/ft)
- α - side slope angle of embankment

Figure 9 depicts these variables for a general flow situation. The gravitational constant is contained in the permeability term by the relationship (12)

$$k = k_o \rho g / \mu \quad (4.1)$$

where k_o (ft²) is the physical permeability dependent only on the soil characteristics and not on those of the fluid, ρ (slug/ft³) is the fluid mass density, g (ft/sec²) is the gravitational constant, and μ (lb-sec/ft²) is the fluid absolute viscosity. Therefore, k already incorporates the gravitational constant, so g is not necessary as a fundamental variable.

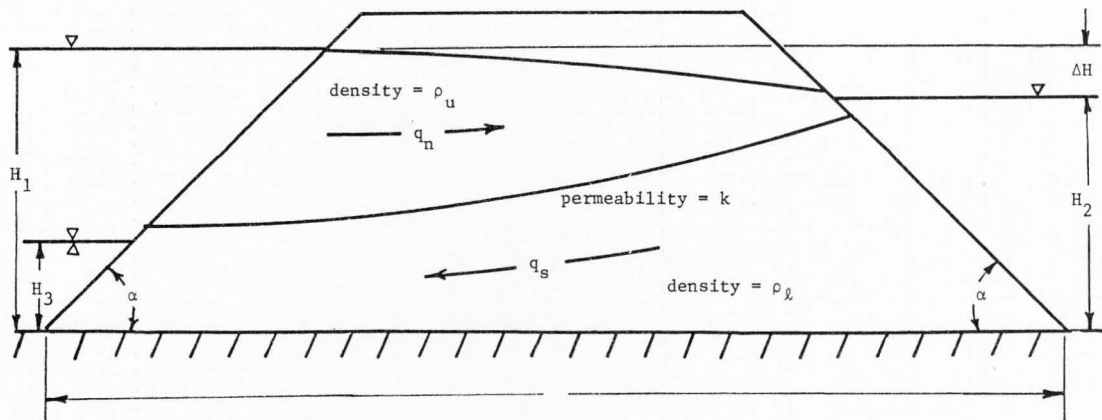


Figure 9. Important variables encountered in this study.

Consideration of continuity suggests the existence of a northside density interface. One would suspect that there must be a layer of less dense brine overlying the near-saturated north brine, but data and sketches in the Waddell-Bolke report have shown no indication of this reality. Therefore, the less-saturated northward flowing brine may quickly mix with the north brine waters, perhaps within the rip-rap over the earth embankment itself, leaving little or no detectable layering on the north side of the embankment. This study, therefore, does not include the interface elevation of the north side as a fundamental variable and assumes that the north lake waters have constant density throughout.

The nine fundamental variables can be non-dimensionalized to six dimensionless parameters. These dimensionless parameters (in parentheses in Equation 4.2) are then used for the data correlation.

$$(q/kH_1) = f \left[(\Delta\rho/\rho_k), (\Delta H/H_1), (H_1/H_3), (W/H_1), (\alpha) \right] \quad (4.2)$$

The first term is the dependent term and the other five are the independent terms.

Since there are so many parameters, it is not possible to formulate a single governing equation for flow rates for this problem. Therefore, a number of graphs have been prepared which encompass the range within which the above dimensionless parameters vary according to the Waddell-Bolke report. The following ranges of values were found for these parameters for the years 1968 through 1972 (Table 1).

Casagrande (2) describes the final design of the rockfill embankment (Figure 10) on which its construction was based, but indicates that many variations from this section were developed. For modeling purposes a 1:1

Table 1. Typical ranges of values for dimensionless parameters.

Dimensionless Parameter	Range
$\Delta\rho/\rho_k$.05 - .1
$\Delta H/H_1$.5 - 2.0
H_1/H_3	4. - 6.
W/H_1	3.5 - 4.5
α	1:1 - 1:3*

* $\alpha = 45^\circ$ or 1:1 is the only slope employed in this analysis

slope was chosen for the innermost semipermeable core. Tracer studies taken in the fill indicated essentially no flow of fluid in the lower sand and gravel base layer. Apparently, clay and evaporates cemented this layer to make it essentially impermeable (24). This cementation may also serve to decrease the pore size dimensions in the rockfill sections giving them their low values of permeability. The exchange of brines between the north and south sections of the lake occurs only in the upper core of the embankment. Therefore, a study of the embankment can be limited to a section such as that depicted in Figure 9.

Since Darcy's law is assumed valid in this analysis, flow rate is directly proportional to the value of permeability (assuming all other parameters are kept constant). For ease in computation, the permeability was chosen to be equal to 1.0 ft/sec. If k was chosen to be very small ($<10^{-2}$), numerical round-off error became more pronounced resulting in erratic numerical solutions.

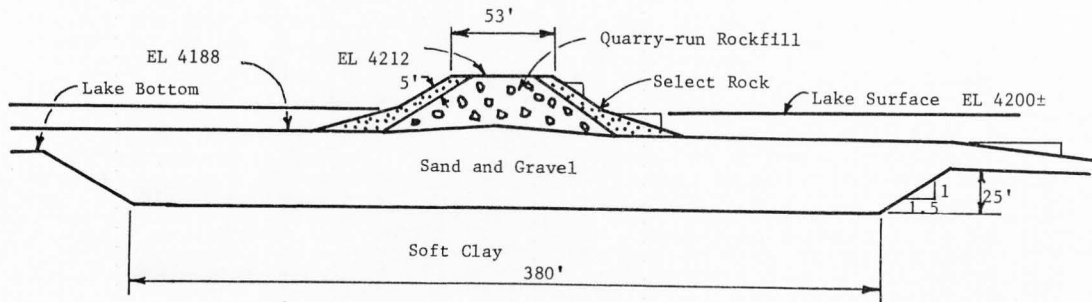


Figure 10. Final construction specifications for Southern Pacific Railroad causeway fill (from Casagrande (2)).

CHAPTER V
RESULTS AND DISCUSSION

Two Domain Problem

In order to keep the number of dimensionless parameters to a minimum, it was decided to model only a single side slope angle for the earth embankment. A forty-five degree angle was chosen for ease in calculating the nodal geometry of the domain. The side slopes of the actual Salt Lake causeway are variable across its length and may be as flat as 3 to 1 in some sections. Modeling a single value of side slope allows one to deal with five dimensionless parameters rather than six; a great reduction in variable correlation.

To obtain numerically convergent solutions, it was necessary to use a large number of elements with a high degree of refinement near all outside surfaces and at the density interface. The final mesh chosen to represent the causeway had ninety-six elements arranged in six rows and eight columns in each of the two single-density regions. Figure 11 illustrates a qualitative view of this mesh.

The two domains were originally generated by mapping the entire domain from a single 8-node serendipity element. During the iterative process nodal points along the density-interface, free surface, and base of the total domain were saved and used to regenerate the nodal positioning in both the upper and lower domains. This technique allowed the density-interface and free surface to take shapes having a greater-than-quadratic variation in the overall sense. Each individual element side was still no greater than quadratic because of the use of quadratic isoparametric quadrilateral elements incorporated in the analysis.

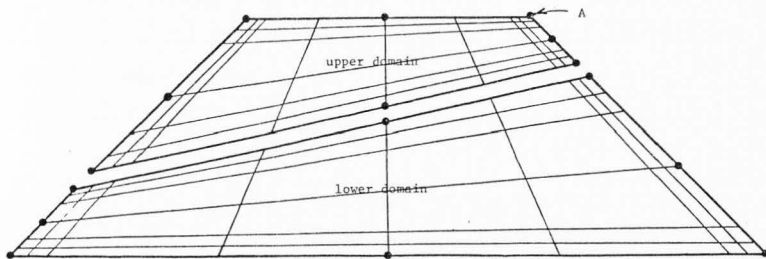


Figure 11. Visual representation of two domain mesh generated by automatic mesh generator.

Ideally, elements should have well-proportioned shapes. That is, large angles within an element should be avoided. Failure to do so may lead to poor results. The mesh used was not ideal, but was found to provide continuity of fluid between the north and south sides of the domain ranging from three to four percent for most solutions. Larger continuity errors were observed only when flow through the region was very low. It was not possible to formulate ideal elements with automatic mesh generation. Therefore, it was necessary to compromise between ideal element shapes and computational effort by "idealizing" the mesh as much as possible within the limitations of the automatic mesh generator used.

Note the refinement of the mesh toward the outside edges of each region. These are the areas where the velocity gradients are the largest and where element distortion is the greatest. In order to obtain accurate velocity calculations in these areas and reduce the effect of the distorted elements, it was necessary to greatly refine the domain mesh. For example, the element labeled "A" had approximate dimensions of .05 ft. x .05 ft.

This model assumes that the fill is isotropic. That is, that the permeability at a given point is equal in all directions. Because of the manner in which the fill was originally constructed, it is possible that the fill may either be anisotropic, favoring flow in the horizontal direction, or it may have two or more isotropic (or anisotropic) layers of differing permeabilities. The present model can handle a special case of anisotropy readily, but cannot model layers of varying permeabilities in its present state. The mathematical and numerical theory would remain unchanged, but it would be necessary to incorporate some triangular elements to model the new geometry. The quadrilateral elements used in this analysis would become too distorted for some of the corners which the new geometry would include. The need for such an alteration in the present model cannot be justified until more field data is collected.

Figures 12 through 17 illustrate the relationships between the five of the six dimensionless parameters described earlier. There are two sets of plots for both northward and southward flows. The first two (Figures 12 and 13) depict that set of conditions acting when the ratio of embankment width, W , to southside lake surface depth, H_1 , is a maximum for the years 1968-1972; the second two (Figures 14 and 15) show those conditions when this ratio (W/H_1) is a minimum on the lake for the same years.

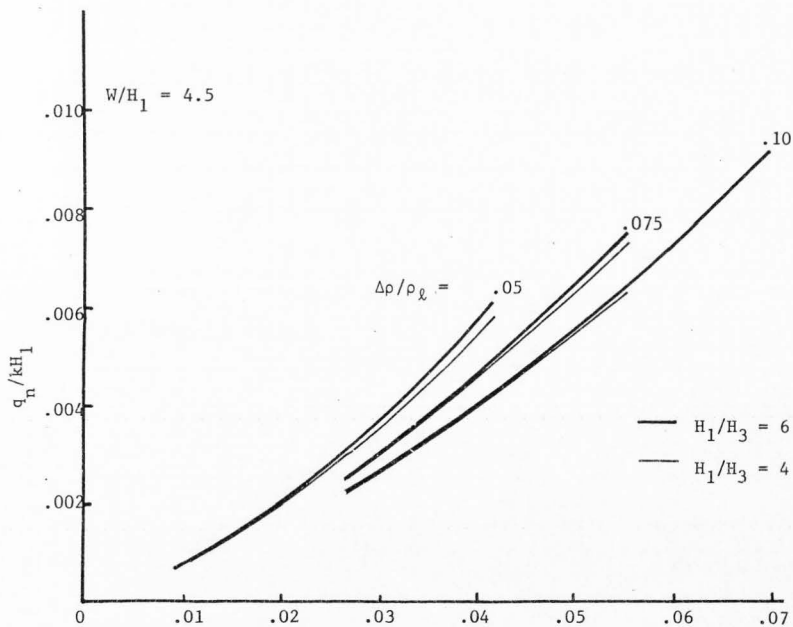


Figure 12. Northward flows for highest W/H_1 ratio observed between 1968 and 1972, and $\alpha = 1:1$.

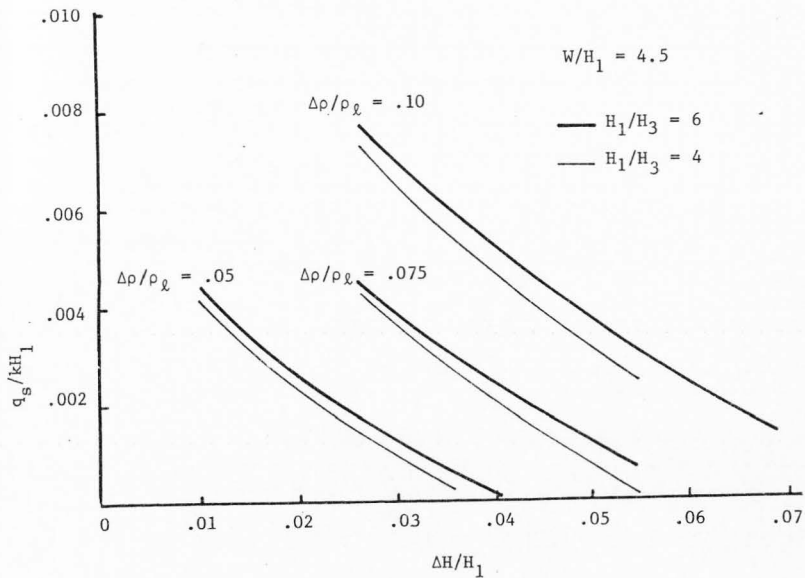


Figure 13. Southward flows for highest W/H_1 ratio observed between 1968 and 1972, and $\alpha = 1:1$.

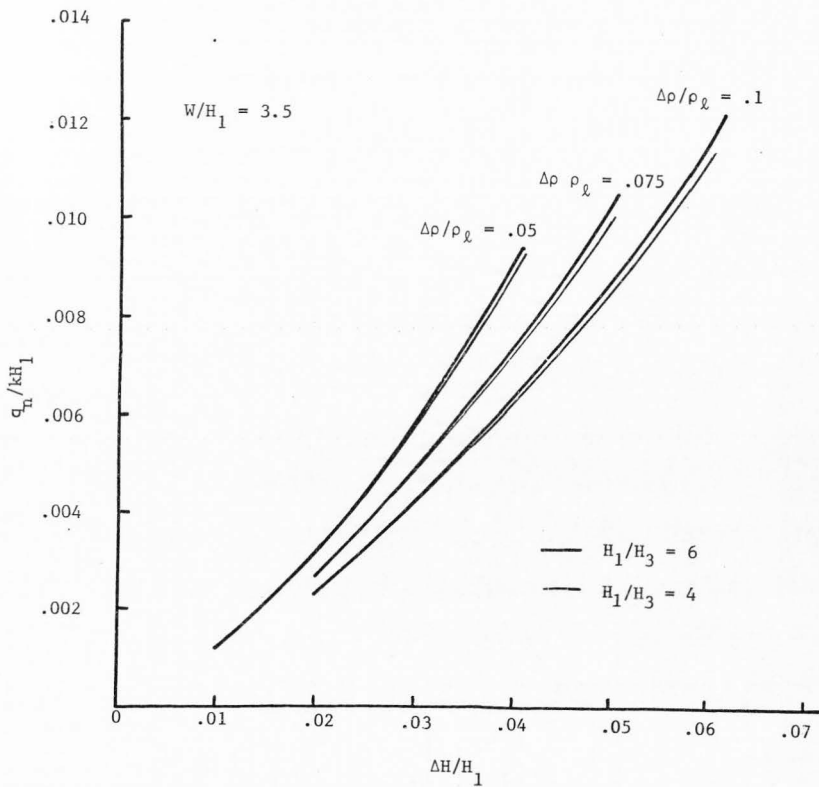


Figure 14. Northward flows for lowest W/H_1 ratio observed between 1968 and 1972, and $\alpha = 1:1$.

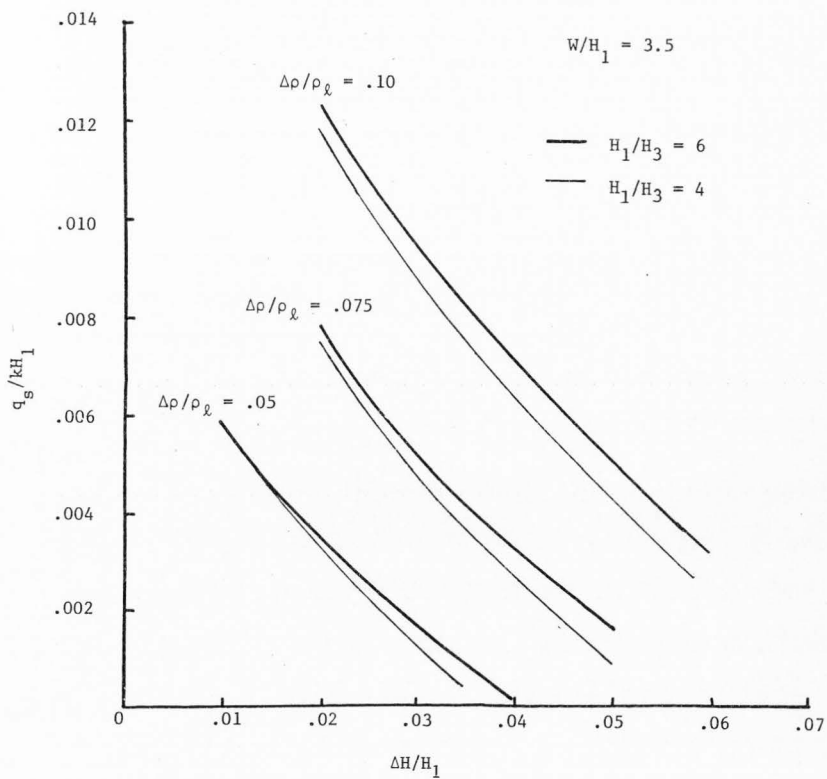


Figure 15. Southward flows for lowest W/H_1 ratio observed between 1968 and 1972, and $\alpha = 1:1$.

For instance, Figures 12 and 13 show that if the earth embankment to be modeled has an effective length ratio (i.e. W/H_1) of 4.5, an H_1/H_3 ratio of 6, with a head drop ratio (i.e. $\Delta H/H_1$) of .022, and a fluid density ratio (i.e. $\Delta\rho/\rho_g$) of .05, the model predicts equal northward and southward flow ratios (q_n/kH_1 and q_s/kH_1 , respectively) of .0024. For a typical value of H_1 of 25 feet and a value of .25 ft/sec for k , this would be a flow rate of .015 ft³/sec per foot of embankment length for either the northward or southward flow. If the proposed section can be considered an average cross section for the total 12.2 miles of the causeway, the total flow through the causeway would be approximately 1000 ft³/sec.

Increasing W/H_1 results in decreasing values of q/kH_1 for both northward and southward flows. The result is depicted in Figures 16 and 17. This essentially states that increasing the effective length of porous media through which a fluid must flow, results in a decrease in the rate of flow.

Figures 18 and 19 indicate the effect that the side slope angle has on the flow rates. It appears that decreasing the side slope decreases southward discharge greatly, while simultaneously decreasing northward discharges to a lesser degree. These two graphs indicate the importance of obtaining a good representative cross section of the embankment before an accurate prediction can be made of actual discharges through the railroad causeway on the Great Salt Lake.

A number of visual generalizations can be ascertained from observing Figures 12 through 17 which satisfy intuitive expectations.

1. Northward flows increased with increasing head drop (ΔH) across the free surface.

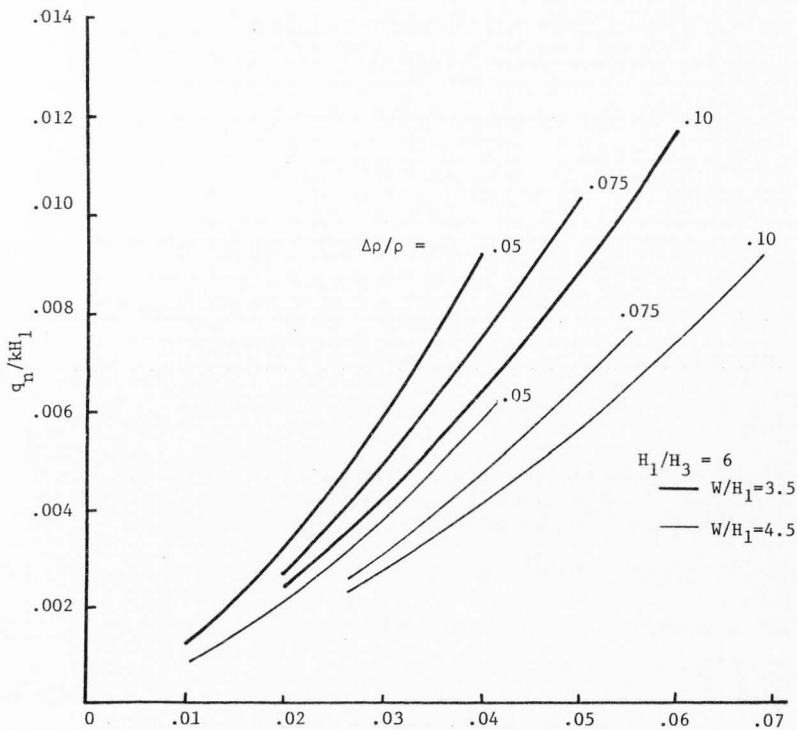


Figure 16. Variation of northward flow with W/H_1 ($\alpha = 1:1$).

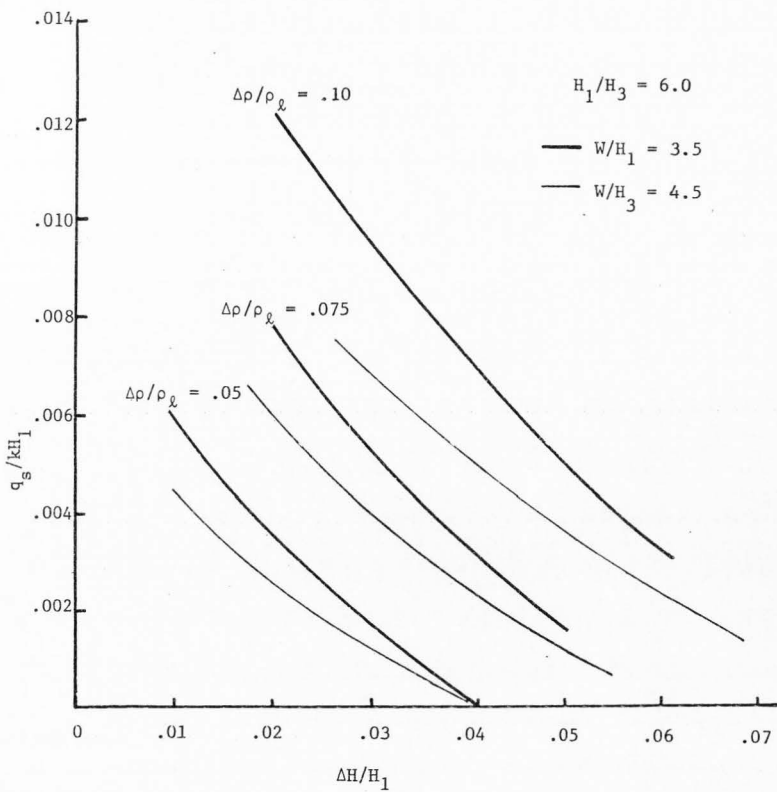


Figure 17. Variation of southward flow with W/H_1 ($\alpha = 1:1$).

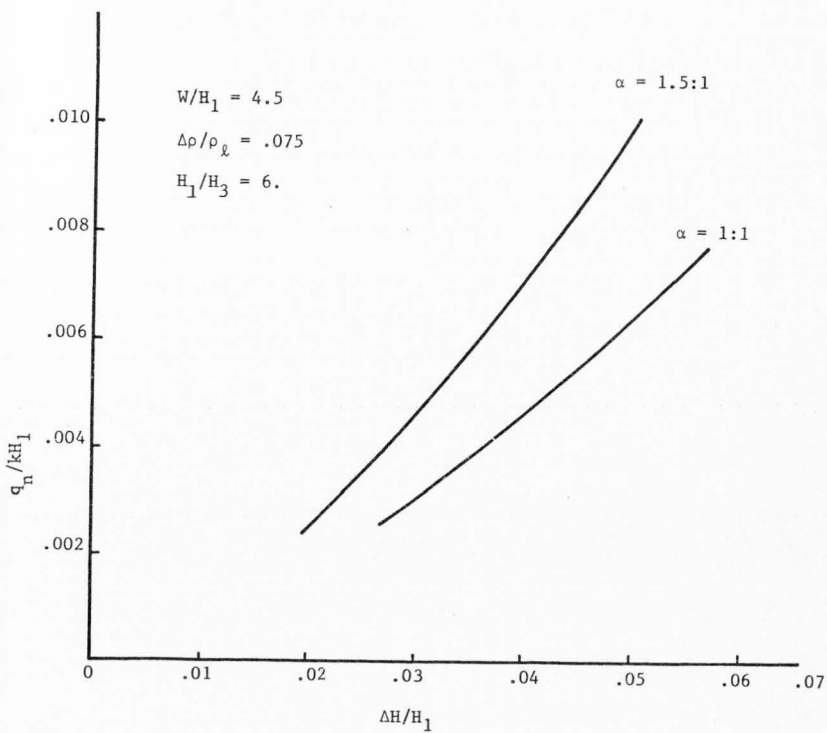


Figure 18. The effect of side slope angle (α) on northward discharges.

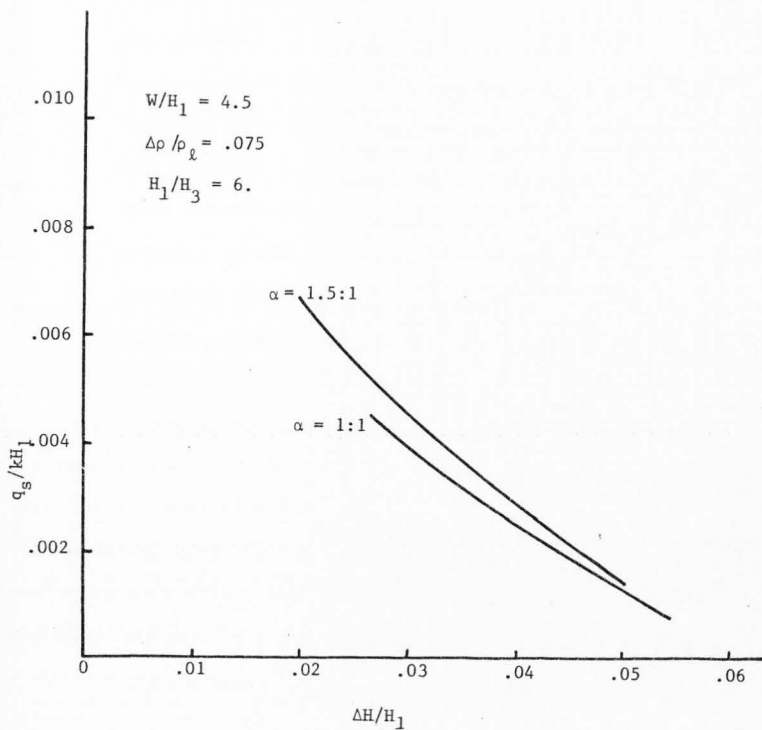


Figure 19. The effect of side slope angle (α) on southward discharges.

2. Southward flows decreased with increasing head drop across the free surface.
3. Northward flows increased for decreasing density differences.
4. Southward flows decreased for decreasing density differences.
5. Both northward and southward flows increased for increasing ratio of southside lake surface elevation to southside density-interface elevation (H_1/H_3).
6. Increasing the ratio of embankment width to southside surface elevation (W/H_1) decreased both northward and southward flow rates.

Item 5 above apparently indicates that decreasing the outlet area for the southward flow, H_3 , has less effect on this flow than the driving head of the density flow (i.e. H_2-H_3 in Figure 9).

Northward flows are most greatly affected by the head drop ratio across the free surface ($\Delta H/H_1$) and the ratio of embankment width to southside lake surface elevation (W/H_1) (Figure 13). The density-difference ratio ($\Delta\rho/\rho_\ell$) had only moderate affect on these flow rates (Figures 12 and 14). The southward flows were affected mainly by the head drop ratio and the density-difference ratio (Figures 13 and 15). The ratio W/H_1 had only moderate affects on southward flow rates (Figure 17). The stratification ratio, H_1/H_3 , had very little affect on the flow rates over the range of parameters tested.

Figures 13 and 15 show that it is possible to cut off the southward flow by either increasing $\Delta H/H_1$, decreasing $\Delta\rho/\rho_\ell$, or increasing W/H_1 sufficiently. If a hypothetical problem is posed beyond these limits, erratic flow rates and density-interface geometry result due to the fact

that a mathematically ill-posed problem results. The numerical model developed in this analysis cannot accommodate wedge flow situations. For instance, Figure 13 shows that if the flow situation is such that the density difference ratio is .05, the effective length ratio is 4.5, and the ratio, H_1/H_3 is 6., then the southward flow is completely cut off when the free surface head drop ratio is .042. For an average value of H_1 of 25 feet, this would be a head drop across the causeway of approximately one foot.

Figures 20 through 23 illustrate the various shapes that the density-interface can take dependent on the boundary conditions. When conditions are such that the southward flow is larger than the northward flow, the interface varies approximately linearly or slightly concave downward across the domain (Figures 20 and 21). For conditions which make the northward flow larger than the southward flow, the shape of the interface is concave upward increasing in curvature as the southward flow approaches zero (Figures 22 through 23).

Convergence

The rate of convergence was dependent on the initial approximations of the locations of the free surface and density interface, but the final flow configuration for a chosen set of embankment variables was shown to be independent of the initializing geometry. Straight lines were initially assumed for both. For the free surface this line extended from the lake surface elevation on the south side of the embankment to the lake surface elevation on the north side. The initial density-interface location extended from the density-interface elevation of the south lake waters at

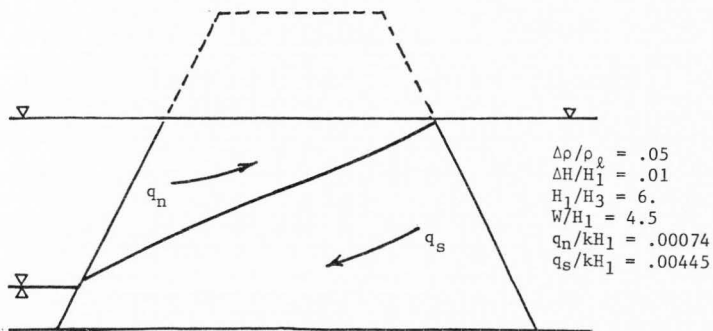


Figure 20. Visual representation of flow when $q_s > q_n$ (vertical exaggeration $2x$).

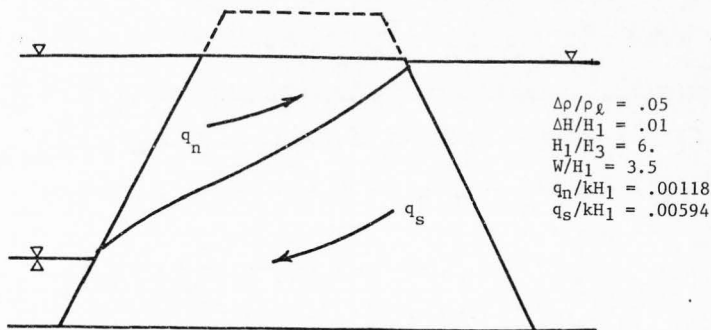


Figure 21. Visual representation of flow when $q_s > q_n$ (vertical exaggeration $2x$).

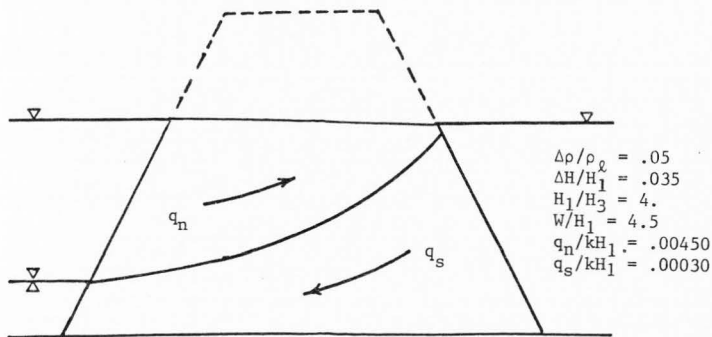


Figure 22. Visual representation of flow when $q_n > q_s$ (vertical exaggeration 2x).

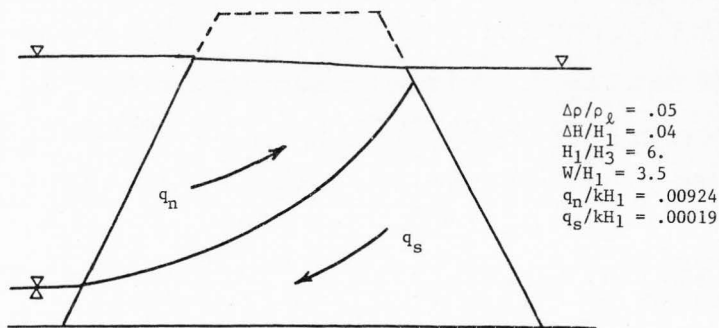


Figure 23. Visual representation of flow when $q_n \gg q_s$ and $q_s \sim 0$ (vertical exaggeration 2x).

the embankment edge to a point on the north side of the earth embankment approximately one vertical foot below the northside lake surface elevation. Recall that all of the brine in the north portion of the lake was considered uniform with no stratification. This initial location was chosen because it represented the approximate final site found in a number of initial experimental numerical solutions.

Using this initial approximation, there were basically two methods used to analyze numerical convergence for this study.

1. Observing the variation of calculated flow rates with the number of iterations and,
2. Observing the largest variation in the free surface and density-interface adjustments with the number of iterations.

A typical problem was run for twenty-three iterations to observe both of these convergence methods.

Figure 24 depicts the convergence of northward flow with iterations. Convergence within the accuracy of the mesh used resulted in approximately five iterations. The flow rates fluctuate within $.003 \text{ ft}^3/\text{sec}/\text{ft}$ thereafter. Figure 25 shows the same sort of convergence for southward flows. Convergence, in this case, has essentially been reached in two iterations varying within $.002 \text{ ft}^3/\text{sec}/\text{ft}$ thereafter.

Figure 26 illustrates the convergence of the density-interface location with iterations. The rate of convergence is very fast for the initial iterations, then approaches the final solution in a more gentle fashion.

The convergence of the free surface was very rapid as shown in Figure 27. Total convergence (within a very small tolerance) was reached within seven or eight iterations.

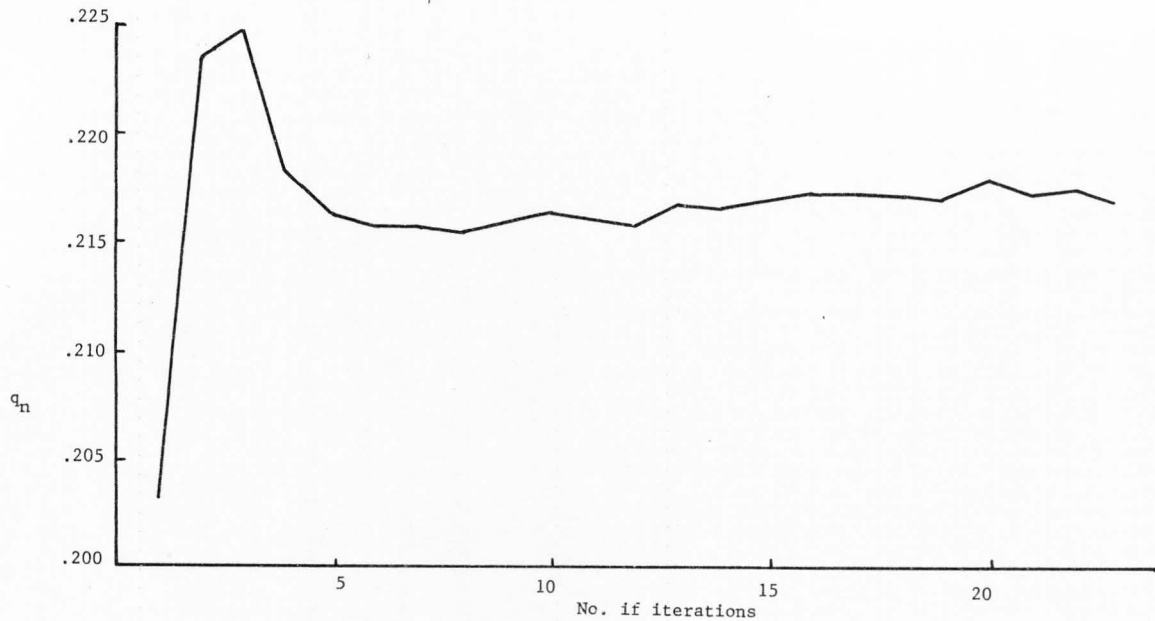


Figure 24. Convergence of northward flow rate with iterations.

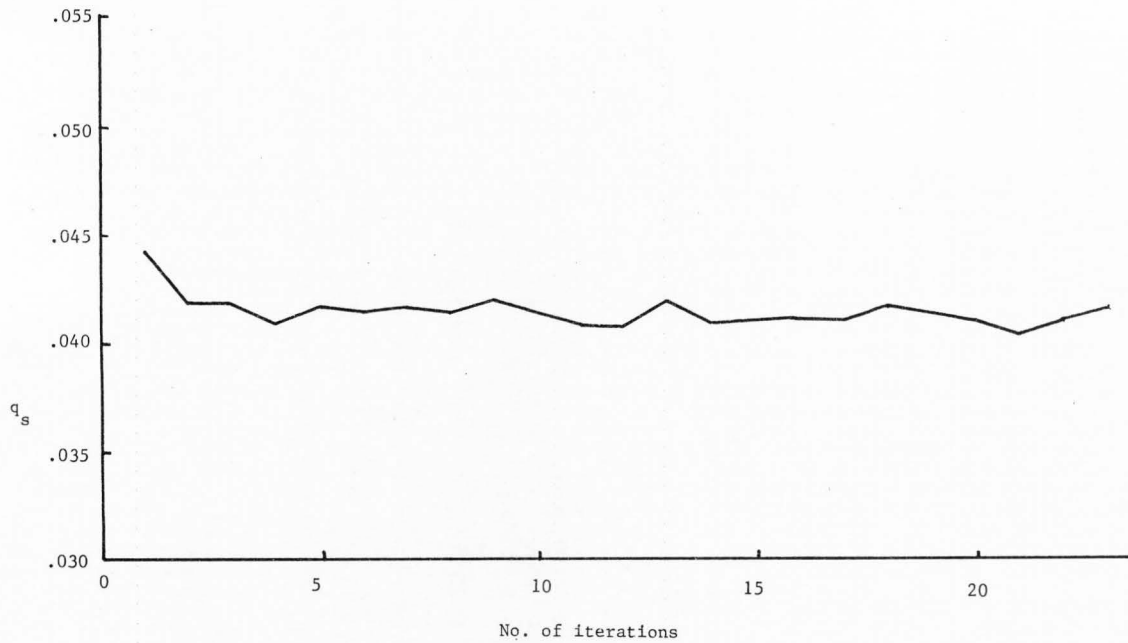


Figure 25. Convergence of southward flow rate with iterations.

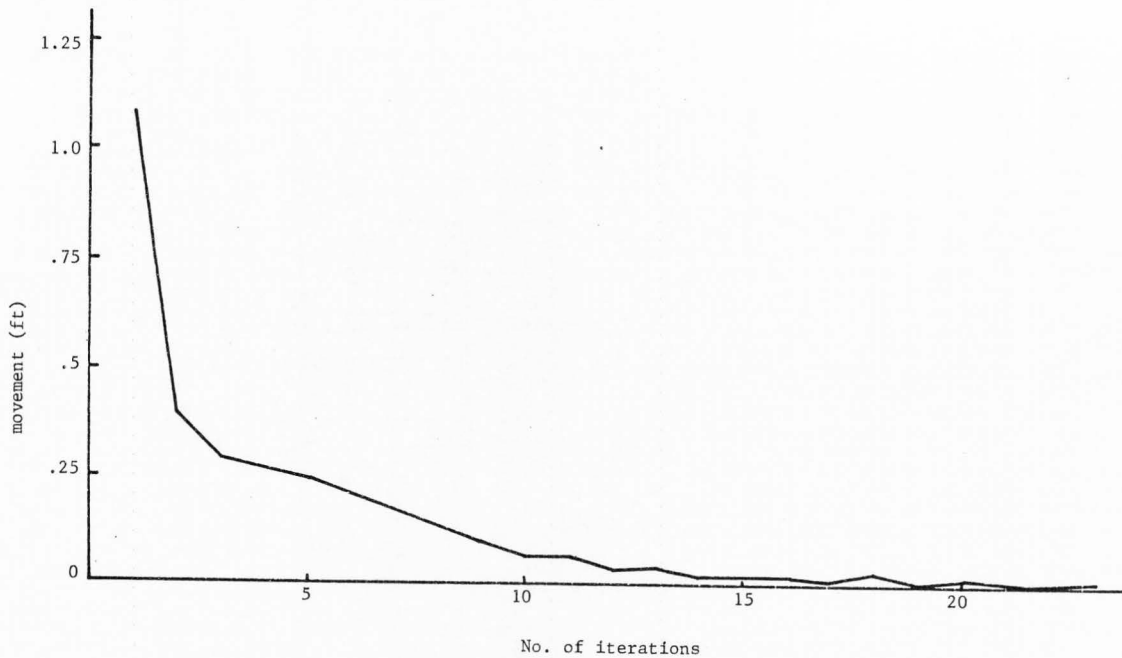


Figure 26. Convergence of maximum density-interface movement with iterations.

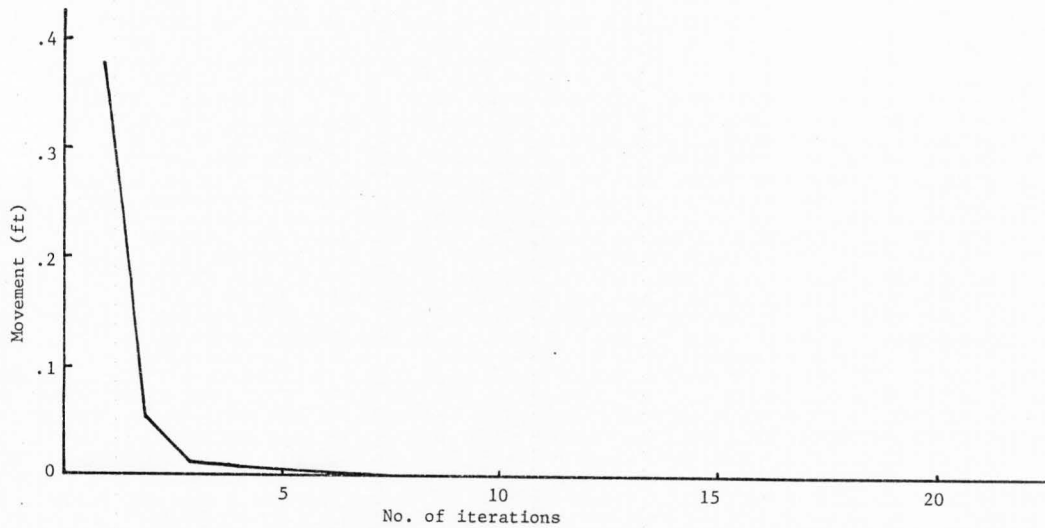


Figure 27. Convergence of maximum free surface movement with iterations.

To avoid excessive computer costs and yet still obtain accurate solutions, it was decided that the maximum allowable normal movement for either the free surface or the density-interface between iterations would be .1 ft. This allowable tolerance enabled a solution to be reached for a given problem within ten iterations using the mesh refinement described previously.

Length of seepage face

As might be expected, the free surface seepage face (located along BC in Figure 28) increased in length for higher values of ΔH across the earth embankment. This length was very small varying between .01 and .07 feet, essentially negligible compared to the dimensions of the total embankment.

The seepage face located along CD in Figure 28, had somewhat longer lengths varying from .3 to 2.0 feet. This length increased with increasing values of ΔH . Decreasing the density-difference ratio, $\Delta\rho/\rho_\ell$, increased the length of CD.

The length of the seepage face located along EF in Figure 28 varied from .01 to .4 feet. It increased in length for increasing values of $\Delta\rho/\rho_\ell$ and decreased in length for increasing values of ΔH .

Special techniques

The nodal movement of the free surface was performed using the following equation:

$$\Delta y_i = \gamma p_i / \rho g \quad (5.1)$$

where Δy_i is the normal movement of the i th node on the free surface, p_i is the calculated pressure at that node, ρ is the density of fluid within

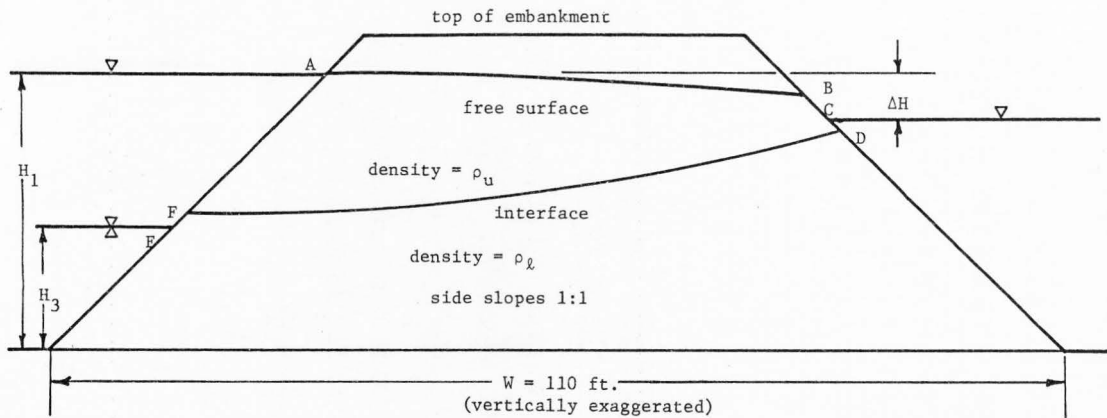


Figure 28. Important variable values and points used in this analysis.

the element, g is the gravitational constant, and γ is a convergence weighting parameter to be chosen empirically with experimental test runs of the program. If γ is chosen too high the location of the free surface will oscillate too violently for convergence to be reached. If it is chosen too low convergence will be much too slow for program efficiency.

Nodal points along the interface were adjusted based on the pressure differences found between the pressures calculated in the upper and lower domains at a given point. The following equation was used to perform this:

$$\Delta y_i = \beta \frac{(p_l - p_u)_i}{\rho_{av} g} \quad (5.2)$$

where Δy_i is, again, a normal adjustment at node i , $(p_l - p_u)_i$ is the difference between pressures calculated in the lower and upper domains at node i , ρ_{av} is the average density of fluid across the interface (i.e. $(\rho_l + \rho_u)/2$), and β is a convergence parameter to be experimentally determined.

For mathematical reasons, it is required that all corner nodes in these boundary value problems have Dirichlet boundary conditions (i.e. the value is specified). The above mentioned relocation schemes cannot move these Dirichlet nodes. Therefore, it was necessary to develop a projection, or extrapolation, scheme to relocate these end points. It was found that projecting these points linearly through the coordinates of the two adjacent element corner nodes, which were relocated, was most productive.

In order to aid in convergence to a unique solution with a minimum number of iterations a number of programming techniques were employed on the end elements of the free surface and the density-interface. In two

of the problems, the northside end of the free surface had a tendency to curl up. In reality, this cannot be the case. This phenomenon may have been caused by the proximity of very small elements to elements of much larger dimensions. It was corrected by enforcing the restriction that a point on the free surface located to the north of an adjacent point must have an elevation less than or equal to that of its southern neighbor (free surface must continually slope downward, or be at worst horizontal, in the direction of flow).

The northern end of the density interface also had a tendency to curl up in some of the problems posed. In actuality, the interface may take on such a shape, but it caused erratic flow rates to be calculated due to severe element distortion. The model was, therefore, constrained to prevent this from occurring.

Applicability of model to Great Salt Lake

This model study is directed toward simulating the earth embankment of Great Salt Lake. Therefore, the range of parameters used in this analysis were chosen to bracket the spread of values which occurred in reality. Because of the numerous parameters involved and the scarcity of useful causeway data, it was not possible to rigorously verify the present model. The program developed in this study does provide similar relationships to those of two previous model studies performed by Lin and Lee (17) and Cheng (4), although the parameters they used were outside the range of values actually occurring on the lake.

Lin and Lee (17) constructed a Hele-Shaw model to investigate stratified bi-directional flow. Their results are shown as the dashed

line in Figure 29. This figure also contains similar plottings performed with information obtained from the program constructed in this study.

It should be noted that Lin and Lee allowed both H_1/H_3 and W/H_1 to vary in their model study. Since these parameters affect the rate of flow, their flow rate curve cannot be directly compared to those developed in this finite element analysis. However, the general trends apparent in the curves can be compared. Also note that although the density-difference parameter $\Delta\rho/\rho_\ell$ used by Lin and Lee was much higher than that occurring in Great Salt Lake, the general shape of the curves are similar. Increasing $\Delta\rho/\rho_\ell$ tends to flatten the curves toward that obtained by Lin and Lee. The other dimensionless quantities (i.e. H_1/H_3 and W/H_1) are relatively unimportant in this qualitative comparison, but would have to be investigated for a comprehensive comparison between the Hele-Shaw model and the computer program constructed in this study.

In Cheng's analysis, the findings were plotted as the ratio q_s/q_n , against the density-difference ratio. The comparison of the present study to Cheng's findings could again be only qualitative because of Cheng's employment of northside stratification. The dashed line in Figure 30, represents a portion of the results from Cheng's report. The solid line is that derived from this study for identical parameter values and geometry of the fill. The two curves have the same basic shape. The difference between them appears to be a function of the northside stratification used in Cheng's analysis. Assuming that the northside fluid is unstratified causes a back pressure on the north side of the fill. This back pressure may be the cause of the cut off which occurs from the program analysis at $\Delta\rho/\rho_\ell$ approximately equal to .025. It is, therefore, important to

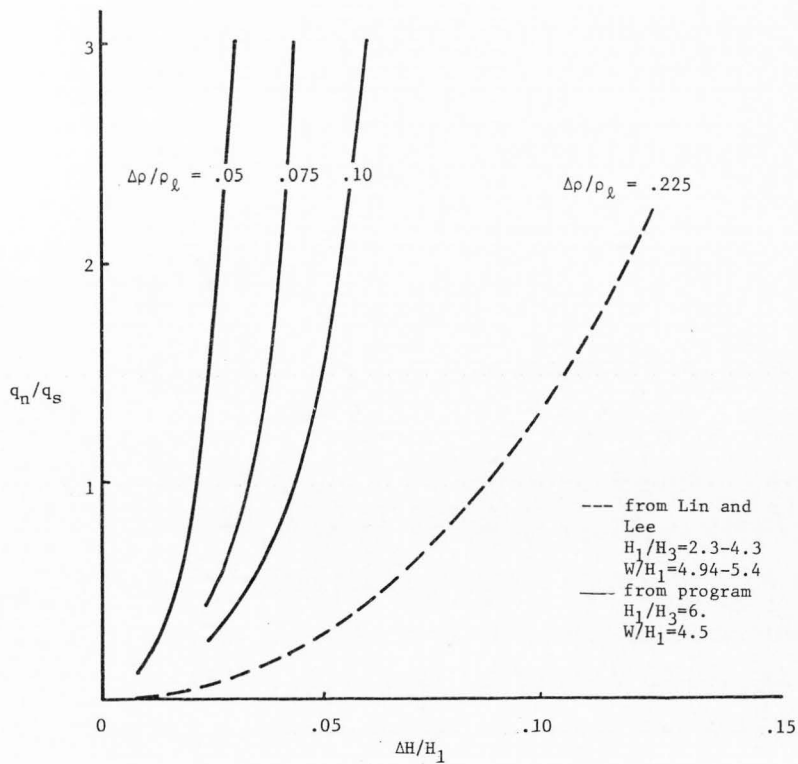


Figure 29. Comparison of constructed model with that of Lin and Lee (17).

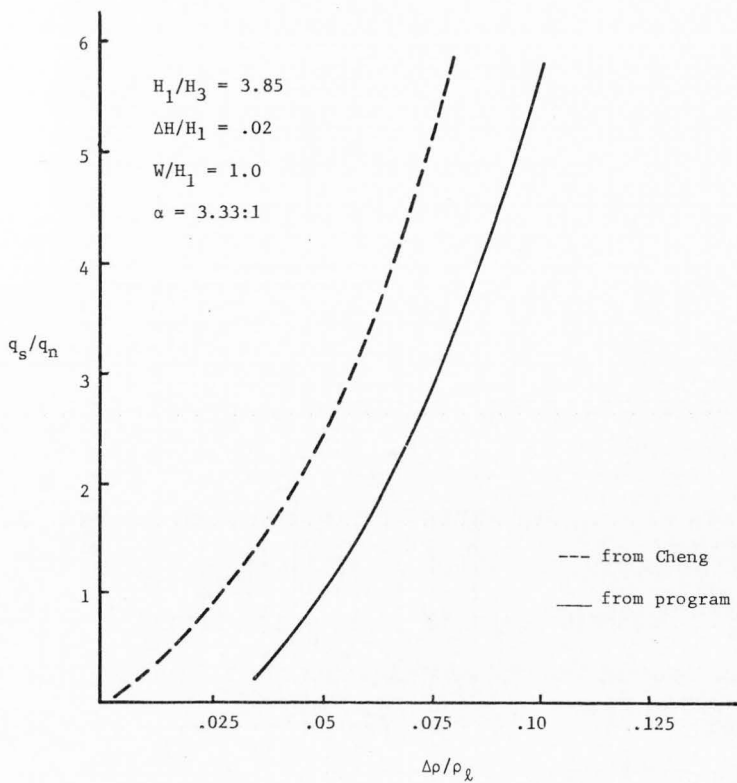


Figure 30. Comparison of constructed model with that of Cheng (4).

establish whether the waters on the northside of the embankment are stratified or not. This can only be based on empirical data, of which there is little at present. Previous data and studies on the embankment do not indicate any stratification on the north side, but before this assumption can be verified more data is needed.

Very little field data has been obtained which is pertinent to this study. The Waddell-Bolke report contains sufficient information concerning surface elevations and densities of the north and south portions of the lake, but has very little in the way of flow rates through the fill. Only one complete set of flow rate data was obtained through this source. It should be observed that the flow rates calculated from this source may not be totally accurate due to the inexact nature of field permeability tests. Tracer studies of north and south flows were taken during May-June 1972, and northward flow rates were determined for August-September 1971. The pertinent information collected from these tests is shown in Table 2.

Through utilization of the various graphs presented in this report and using the dimensionless variables listed above, the dimensionless variable, q/kH_1 , could be ascertained for both northward and southward flows. The necessary value of permeability could be roughly estimated by comparing the flow rates calculated by Waddell and Bolke to those calculated by the computer program as shown in Table 3.

A computer run was also made using the lake parameters for the May-June 1972 data with 1.5:1 side slopes instead of the 1:1 slope used in the above calculations. The value for permeability calculated as in the preceding manner was found to be approximately 0.5 ft/sec.

Table 2. Variables pertinent to causeway flow collected by Waddell and Bolke (24).

	May-June 1972	Aug.-Sept. 1971	Units
H_1	29	27	ft.
ΔH	1.55	.98	ft.
H_3	6.5	3.75	ft.
W (assumed)	110	110	ft.
ρ_λ	2.328	2.359	slugs/ft ³
ρ_u	2.109	2.157	slugs/ft ³
q_n	.07	.025	cfs/ft
q_s	.021		cfs/ft
$\Delta\rho/\rho_\lambda$.094	.086	--
$\Delta H/H_1$.053	.036	--
H_1/H_3	4.46	7.2	--
W/H_1	3.79	4.07	--

Table 3. Permeability calculations deduced from comparison of program flow rate calculations and actual lake values.

Date	Direction	q_c/kH_1^2	q_c/k (ft ² /ft)	q (cfs/ft)	k (ft/sec)
May-June 1972	Northward	.009	.261	.07	.268
May-June 1972	Southward	.0031	.0928	.021	.233
Aug.-Sept 1971	Northward	.0045	.1242	.025	.201
Average - .234					
q - from Waddell and Bolke (24)					
q_c - from program					

The above values for permeability lie well within the range of permeability values estimated in the Waddell-Bolke report. Individual permeability values calculated by Waddell and Bolke varied erratically from .08 ft/sec to 2.1 ft/sec. Since the permeability value has a very large influence on the calculated flow rates, it is imperative that a more accurate value of this quantity be found if this model is to be used as a predictive instrument applicable to Great Salt Lake. If more data on flow rates through the earth embankment is procured, it may be possible to deduce a more confident value of permeability by employing the method shown in Table 3.

The theoretical equation which this model solves is based on Darcy's law. Darcy's law is valid only for flows having low Reynold's numbers. Harr (12) states that the upper limit of the Reynold's number for laminar flow is between 1 and 12. Using an average value of permeability calculated above (i.e. 375 ft/sec) and information from the data collected during May-June 1972, it is possible to roughly estimate the Reynold's number describing flow in this analysis.

$$\text{Reynold's no.} = \frac{V D \rho}{\mu}$$

where

- D = average diameter of sand particles
- V = average fluid velocity
- ρ = density of fluid
- μ = coefficient of viscosity

The particle diameter can be taken as that of coarse sand, approximately 3/8 in., or .0313 ft. Based on the assumed dimensions of the fill and the northward flow rate (.07 ft³/sec/ft) the average velocity was

found to be .007 ft/sec. If the density of the brine and the viscosity of saturated brine are used, the Reynold's number was found to equal 13. This high value indicates the onset of turbulent flow conditions, but the values used to calculate this Reynold's number were for the highest water period of the year. The obvious question then arises as to whether the assumption that Darcy's law applied to the embankment flow is valid. It should be noted, however, that the value calculated was within the range of the highest Reynold's numbers the flow through the earth embankment is likely to see. The validity of Darcy's assumption in this analysis can only be ascertained through more empirical data.

Single Domain Problem

It was not possible to obtain a converging solution for a flow problem when posed as a single domain. The discontinuity of velocities at the density-interface was too erratic to allow a unique location of the interface to be found.

The mesh rearrangement and refinement procedures employed did not aid in obtaining better solutions which suggests that:

1. If a converging solution is possible, a special weighting technique must be devised to aid in uniform convergence or,
2. A continuous velocity formulation is necessary such as that described by Pinder and Gray (20).

It may still be possible to obtain solutions useful for engineering purposes using the single domain formulation employed in this study, but much more work is necessary and must be left to later studies. The difficulties encountered in the single domain method pointed this work

in the direction of formulating the problem using two domains, each having a constant density fluid.

CHAPTER VI

CONCLUSIONS AND RECOMMENDATIONS

Previous model studies dealing with stratified bi-directional flow through porous media do not consider many of the important parameters involved to properly model realistic problems. This study performs a more comprehensive treatment of the parameters relative to predicting flows through the causeway fill of Great Salt Lake. It was found that such problems could be more fully described by considering the following parameters:

$\Delta\rho/\rho_\ell$ = ratio of density difference to density of southward flowing fluid

$\Delta H/H_1$ = ratio of drop in lake surface elevation to southside lake surface elevation

W/H_1 = ratio of embankment width to southside lake surface elevation

H_1/H_3 = ratio of southside lake surface elevation to northside density-interface elevation

q/kH_1 = ratio of flow rate (either north or south) to the product of field permeability with southside lake surface elevation

α = side slope angle of embankment

Although rigorous verification could not be performed, the finite element model developed in this study proved to generate credible estimates for flow rates occurring through the causeway fill of Great Salt Lake. Continuity checks performed along the north and south sides of

the domain of flow showed that net flows differed by only 3 to 4 percent across the embankment for the finite element mesh used. Flow rate curves produced with the model had similar shapes to those developed by earlier investigations which used Hele-Shaw models for either data collection or model verification. The curves developed in this and the two previous investigations appeared to originate from the same family of curves with discrepancies resulting from parameter differences and the assumption of no stratification on the north side of the embankment.

It was shown that side slope angle of the embankment had a major effect on northward flows and a lesser effect on southward flows. It was also found that assuming the northern waters to be unstratified has a major effect on flow rates through the fill. It is, therefore, imperative that more embankment data be collected to establish representative geometries and to determine whether the north lake waters are stratified near the embankment sides.

Comparison of results from this model (for side slopes of 1:1 and no north side stratification) to actual data collected on the Great Salt Lake embankment indicated solutions within ten or fifteen percent accuracy could be calculated using a homogeneous, isotropic permeability value of .23 ft/sec for the earth embankment. This value was found using only three field data points, so can only be considered a very rough estimate. Using this value of permeability and an average southside lake surface depth of 25 feet, the upper limit of flows for both northward and southward flowing waters appeared to be approximately .09 ft³/sec/ft, or about 6000 ft³/sec for the whole embankment length.

A fairly high value of Reynold's number was calculated using rough estimates and data taken from the highest flow rate period on the embankment. Whether Darcy's law is valid for these flow rates can only be established with more field data taken on the embankment.

It was also found that proper combinations of lake parameters could totally cut off the southward density flow. This occurred for free surface head differences between 1.0 and 2.0 feet, depending on the relative densities of the upper and lower fluids. Lower density differences required less head difference for southward flows to be cut off.

Variations of the important parameters found in this investigation affected northward and southward flow rates in differing manners. Northward flows increased for (1) increasing head drop across the fill, (2) increasing southside lake surface elevation, and (3) decreasing density difference between the northward flowing and southward flows. Northward flows also increased for decreasing elevation of southside density-interface, although, this parameter had little effect in comparison to the above mentioned parameters over the range of values tested. Southward flows increased for (1) decreasing head drop across the fill, (2) increasing southside lake surface elevation, and (3) increasing density difference. Southward flows also increased for decreasing elevation of the southside density-interface, but again, this parameter had a relatively minor effect over the range of values tested.

The model developed in this study adequately simulates those conditions existing in the earth embankment of Great Salt Lake for the scarce field data used in verification. The model is only as accurate as the field data used, so the most important suggestion for further investigation

in this area is to initiate a program for collection of more field data, concerning flow rates through the fill, to verify those calculated by the model. This data could undoubtedly be collected with tracer tests for determining flow rates, both northward and southward through the fill, and field permeability tests for determining an average permeability values. With an adequate number of flow rate tests, it may be possible to deduce a confident value for permeability without performing field permeability tests.

It should also be noted that in the field study analysis by Waddell and Bolke, the northward and southward flows were divided further into those in the west 40% portion of the causeway and those in the east 60% portion. Apparently, they considered the two portions to have sufficient-ly different characteristic properties to warrant separate analyses. The present analysis has assumed the total causeway to be homogeneous, but further field investigation may prove this not to be the case. If the causeway is found not to be homogeneous along its length, then a proper analysis will have to choose a number of representative cross sections and sum up the contributions of each to adequately model flows through the entire embankment length.

It was found that if the problem of stratified bi-directional flow was posed as a single domain analysis, it was not possible to reach a convergent solution with the element mesh generator and dependent variables selected. The velocity discontinuities at the density-interface were too great to allow a unique solution to be found. Dividing the total domain into two constant-density regions provided rapidly convergent solutions.

This method was the one employed to model flow rates through the causeway fill of Great Salt Lake.

LITERATURE CITED

1. Adams, T. C.: "Salt migration to the northwest body of Great Salt Lake, Utah," Science, March 1964.
2. Casagrande, A.: "Role of the 'Calculated Risk' in earthwork and foundation engineering," Jour. of the Soil Mechanics and Foundations Div., ASCE, Vol. 91, No. SM4, July, 1965.
3. Casagrande, A.: "Seepage through dams," Boston Soc. Civ. Engr. Contributions to Soil Mechanics, 1925-1940, pp. 295-336, 1937.
4. Cheng, R. T. and M. Hu: "Study of fluid movements through causeway," Jour. of the Hydraulics Div., ASCE, HY1, Proc. Paper 11076, pp. 155-165, Jan. 1975.
5. Desai, C. S.: "Finite element residual schemes for unconfined flow," Int. Jour. Num. Meth. Engr., Vol. 10, pp. 1415-1418, 1976.
6. Desai, C. S.: "Seepage analysis of earthbanks under drawdown," Jour. of the Soil Mechanics Div., ASCE, SM11, Proc. Paper 9334, pp. 1143-1161, Nov. 1972.
7. Ergatoudis, I., B. M. Ikons, and O. C. Zienkiewicz: "Curved, iso-parametric, quadrilateral elements for finite element analysis," Int. Jour. Solids Struct., Vol. 4, pp. 31-42, 1968.
8. Finlayson, B. A.: The Method of Weighted Residuals and Variational Principles, Mathematics in Science and Engineering, Vol. 87, Academic press, New York, 1972.
9. Finnemore, E. J. and B. Perry: "Seepage through an earth dam computed by the relaxation technique," Water Resources Research, Vol. 4, No. 5, pp. 1059-1067, Oct. 1968.
10. France, P. W.: "An improved finite element technique for the analysis of free surface flow problems," Computers and Fluids, Vol. 3, pp. 149-153, 1975.
11. France, P. W., C. J. Parekh, J. C. Peters, and C. Taylor: "Numerical analysis of free surface seepage problems," Jour. of the Irrig. and Drain Div., ASCE, Vol. 97, IR1, Proc. Paper 7959, pp. 165-178, Mar. 1971.
12. Harr, M. E.: Groundwater and Seepage, McGraw-Hill Book Co., Inc., New York, 1962.
13. Herbert, R.: "Time variant groundwater flow by resistant network analogues," Jour. of Hydrology, Vol. 6, pp. 237-264, 1968.

14. Huebner, K. H.: The Finite Element Method for Engineers, John Wiley and Sons, Inc., New York, 1975.
15. Jeppson, R. W.: "Seepage through dams in the complex potential plane," Jour. of the Irrig. and Drain Div., ASCE, Vol. 94, IRI, Proc. Paper 5835, pp. 23-39, March 1968.
16. Liggett, J. A.: "Location of the free surface in porous media," Jour. of the Hydraulics Div., ASCE, HY4, Proc. Paper 12851, pp. 353-365, April 1977.
17. Lin, A. and S. Lee: "A Hele-Shaw model of seepage flow through the causeway of the Great Salt Lake, Utah," The Great Salt Lake and Utah's Water Resources, Proc. of the first annual conf. of the Utah Section of the American Water Resources Association, pp. 134-141, Nov. 30, 1972.
18. Murphy, G.: Similitude in Engineering, The Ronald Press Co., New York, 1950.
19. Neuman, S. P. and P. A. Witherspoon: "Finite element method of analyzing steady seepage with a free surface," Water Resources Research, Vol. 6, No. 3, pp. 889-897, 1970.
20. Pinder, G. F. and E. O. Frind: "Applications of Galerkin's procedure to aquifer analysis," Water Resources Research, Vol. 8, No. 1, pp. 108-120, Feb. 1977.
21. Pinder, G. F. and W. G. Gray: Finite Element Simulation in Surface and Subsurface Hydrology, Academic Press, Inc., New York, 1977.
22. Shaug, J. C. and J. C. Bruch Jr.: "Solutions of a free surface boundary value problem using an inverse formulation and the finite element method," Jour. of Hydrology, Vol. 26, pp. 141-152, 1975.
23. Taylor, R. L. and C. B. Brown: "Darcy flow solutions with a free surface," Jour. of the Hydraulics Div., ASCE, HY2, Proc. Paper 5126, pp. 25-33, March 1967.
24. Waddell, K. M. and E. L. Bolke: "The effects of restricted circulation on the salt balance of Great Salt Lake, Utah," Utah Geological and Mineral Survey, Jan. 1974.